Universidade Federal do Rio Grande – FURG

Instituto de Oceanografia

Programa de Pós-Graduação em Oceanografia Física, Química e Geológica

UMA VISÃO CIRCUMPOLAR DA PARTIÇÃO DE ENERGIA DA CORRENTE COSTEIRA ANTÁRTICA

RUBENS TORQUATO NETO

Dissertação apresentada ao Programa de Pós-Graduação em Oceanografia Física, Química e Geológica, como parte dos requisitos para a obtenção do Título de Mestre.

Orientador: *Prof. Dr.* MAURICIO MAGALHÃES MATA

Universidade Federal do Rio Grande (FURG), Brasil.

Rio Grande, RS, Brasil

Maio de 2018

UMA VISÃO CIRCUMPOLAR DA PARTIÇÃO DE ENERGIA DA CORRENTE COSTEIRA ANTÁRTICA

Dissertação apresentada ao Programa de Pós-Graduação em Oceanografia Física, Química e Geológica, como parte dos requisitos para a obtenção do Título de Mestre

por

RUBENS TORQUATO NETO

Rio Grande, RS, Brasil

Maio de 2018

TORQUATO, RUBENS

Uma visão Circumpolar da Partição de Energia da Corrente Costeira Antártica / Rubens Torquato. – Rio Grande: FURG, 2018.

Número de páginas 64p.

Dissertação (Mestrado) – Universidade Federal do Rio Grande. Mestrado em Oceanografia Física, Química e Geológica. Área de Concentração: Oceanografia Física.

1. Corrente Costeira Antártica. 2. Fundeio Oceanográfico. 3. Ondeletas. I. Uma visão Circumpolar da Partição de Energia da Corrente Costeira Antártica.

[ATA DA DEFESA]

Agradecimentos

Ao meu orientador, Mauricio Magalhães Mata, por ter aceitado me orientar desde a graduação, sempre com muita atenção e paciência, mostrando os melhores caminhos a seguir.

À minha família, por todo o suporte e apoio em todos os meus passos e pelo amor incondicional.

À minha namorada, Letícia por sempre estar ao meu lado, com muito carinho, pelas longas conversas e companheirismo.

Aos amigos do Laboratório de Estudos dos Oceanos e Clima (LEOC) pelas conversas, ajudas e companhias de embarques.

À Coordenação de Aperfeiçoamento de Pessoal de Nível Superior (CAPES) pela bolsa de estudos concedida, e todos os professores do IO pelos conhecimentos passados desde os tempos da graduação.

Índice

Lista de Figuras da Dissertação

Lista de Figuras do Manuscrito

Lista de Tabelas

Lista de Acrônimos e Abreviações

A

ACC – Corrente Circumpolar Antártica (*Antarctic Circumpolar Current*)

ACoC – Corrente Costeira Antártica (*Antarctic Coastal Current*)

ADCP – Perfilador Acústico de Corrente (*Acoustic Doppler Current Profile*)

AIS – Plataforma de Gelo Amery (*Amery Ice Shelf*)

AP – Península Antártica (*Antarctic Peninsula*)

ASC – Corrente de Talude Antártico (*Antarctic Slope Current*)

AWI – *Alfred Wegner Institute*

B

BAS – *British Antarctic Survey*

B-A S – Mares de Bellingshausen-Amundsen (*Bellingshausen-Amundsen Seas*)

C

CDW – Água Profunda Circumpolar (*Circumpolar Deep Water*)

CN – Cabo Norwegia (*Cape Norwegia*)

CTW – Ondas Costeiras Aprisionadas (*Coastal Trapped Waves*)

D

DRT – Depressão de Drygalski (*Drygalski Trough*)

DSW – Água Densa de Plataforma (*Drense Shelf Water*)

DT – Depressão de Dotson (*Dotson Trough*)

F

FIS – Plataforma de Gelo Fimbul (*Fimbul Ice Shelf*)

FT – Depressão de Filchner (*Filchner Trough*)

I

IO – Oceano Índico (*Indian Ocean*)

K

KOPRI – *Korea Polar Institute*

L

LCDW – Água Circumpolar Profunda Inferior (*Lower Circumpolar Deep Water*)

M

mCDW – Água Circumpolar Modificada (*Circumpolar Modified Water*)

MP – Polínia de Mertz (*Mertz Polynya*)

MT – Depressão de Marguerite (*Marguerite Trough*)

P

PC – Cânion Polarstern (*Polarstern Canyon*)

PNRA –*Programma Nazionale di Ricerche in Antartide*

R

RS – Mar de Ross (*Ross Sea*)

S

SOOS – *Southern Ocean Observing System*

U

UCDW – Água Circumpolar Profunda Superior (*Upper Circumpolar Deep Water)*

U.S. GLOBEC – *U.S. Global Ocean Ecosystem dynamics*

W

WDW – Água cálida Profunda (*Warm Deep Water)*

WPO – Oceno Pacífico Oeste (*Western Pacific Ocean*)

WS – Mar de Weddell (*Weddell Sea*)

WSC – Confluência Weddell Scotia (*Weddell-Scotia Confluence*)

Resumo

A Corrente Costeira Antártica (ACoC) é uma importante componente na circulação do Oceano Austral, que flui *quase* continuamente para oeste, ao redor do continente Antártico, controlando o regime oceanográfico sobre a plataforma continental. A ACoC também atua modulando e pré-condicionando as águas de plataforma que eventualmente atuam na formação da Água de Fundo Antártica, sendo assim uma peça chave na circulação oceânica global e regulação do clima. Desta forma, o presente trabalho investigou aspectos da variabilidade do sistema da ACoC utilizando dados de fundeios oceanográficos ao longo da plataforma continental e talude ao redor do continente Antártico. Os 32 fundeios analisados forneceram uma visão circumpolar da variabilidade temporal e a partição de energia associadas com o sistema da ACoC. A banda da alta frequência (com períodos entre 40 horas e 8 dias) contribuiu significantemente com a partição de energia nas camadas superficial e intermediárias. Esta banda foi atribuída a vórtices e Ondas Costeiras Aprisionadas (CTW), que possuem um importante papel na troca de calor na plataforma continental Antártica. Entretanto, a maioria dos instrumentos foram dominadas pela banda sinóptica (com períodos entre 8 e 20 dias), principalmente devido à presença de um intenso sinal quinzenal, atribuído à influência dos ciclos de maré de sizígia e quadratura. De todos os instrumentos analisados, os fundeios localizados próximos à Depressão de Drygalski, na região do Cabo Adare possuíram a maior quantidade total de energia, com grande dominância do ciclo quinzenal, representando mais de 80% da partição de energia. Com exceção da região do Mar de Ross, as bandas da mesoescala superior (com períodos entre 20 e 50 dias) e inferior (períodos entre 50 e 140 dias) foram mais importantes nos fundeios próximos às depressões, como na Depressão de Filchner (Mar de Weddell), Depressão de Dotson (Mar de Amundsen) e Depressão de Marguerite (Mar de Bellingshausen). As oscilações com períodos maiores do que 140 dias (banda da baixa frequência) dominaram a partição de energia em apenas um instrumento (com 95% de intervalo de confiança), localizado no talude continental próximo à Plataforma de Gelo Fimbul.

Palavras-chave: Corrente Costeira Antártica, Fundeios Oceanográficos, Ondeletas.

Abstract

The Antarctic Coastal Current (ACoC) was investigated using long-term mooring data over the continental shelf and slope around the Antarctic continent. The 32 moorings used in the present study provide an attempt of having a circumpolar view of the temporal variability and energy partition associated with the ACoC system. Wavelet analysis has been used to investigate the main signals of variability and how they vary with time. Most of instruments of the surface and upper intermediate layers had significant contribution from a relatively high frequency band (periods between 40 hours and 8 days) to the energy partition. This band has been linked with eddies and Coastal Trapped Waves (CTW), which can play important roles in the heat exchange across the shelf break. However, the majority of the instruments were dominated by the frequency window we defined as weather band (with periods between 8 and 20 days), mainly due a distinct peak at the fortnightly tidal period, which have been attributed by the influence of the spring/neap tidal cycle. The moorings near Drygalski Trough, near the Cape Adare, had the largest total energy among all instruments, with a great dominance of the spring-neap tidal cycle, representing more than 80% of the energy partition. The upper and lower mesoscale bands (with periods between 20 and 50 days for the first, and between 50 and 140 days for the latter) showed to be more important at the moorings near depressions, such as the Filchner Trough (Weddell Sea), Dotson Trough (Amundsen Sea) and Marguerite Trough (Western Antarctic Peninsula). The oscillations with periods greater than 140 days have dominated the energy partition in only one instrument, positioned at the continental slope near Fimbul Ice Shelf, mainly due to a prominent peak at the semi-annual cycle.

Keywords: Antarctic Coastal Current, moorings, wavelets.

Estrutura da Dissertação

Para obter o título de Mestre pelo Programa de Pós-Graduação em Oceanografia Física, Química e Geológica, é requerido que o aluno realize a submissão de pelo menos um artigo científico como primeiro autor em periódico indexado com corpo editorial. Deste modo, os resultados da pesquisa desenvolvida durante o período de mestrado e a discussão dos mesmos serão apresentados em forma de artigo no corpo da dissertação. Neste sentido, o presente documento é composto de cinco capítulos. No capítulo I será apresentado uma breve introdução sobre a importância da Corrente Costeira Antártica e os trabalhos realizados em seu domínio. No capítulo II, os objetivos a serem alcançados no presente trabalho. O capítulo III traz a descrição dos dados e métodos utilizados no presente trabalho. No capítulo IV, os resultados e discussão serão apresentados em forma de artigo. Os principais resultados e conclusões serão sucintamente descritos no capítulo V. Encerra-se o documento com as referências utilizadas na elaboração do artigo e da dissertação.

Capítulo I: Introdução

I. 1 – INTRODUÇÃO

Os oceanos iniciam seus movimentos por meio da transferência de *momentum*, fluxos de sal e calor em variadas escalas espaciais e temporais, onde a energia é transferida para movimentos de escalas cada vez menores, até que esta seja totalmente dissipada, formando a cascata de energia (e.g. Ferrari & Wunsch, 2009). Portanto, o espectro de energia do oceano é resultado da transferência turbulenta de energia entre diferentes regiões e bandas espectrais. Neste contexto, processos de menores escalas são extremamente importantes, pois eles são responsáveis por manter o oceano em equilíbrio.

O Oceano Austral possui um importante papel na circulação oceânica global que, sem barreiras geográficas na faixa latitudinal do Estreito de Drake, ao sul da América do Sul, conecta as três maiores bacias oceânicas do planeta (Figura 1). Devido à ação dos fortes ventos de oeste e grande fluxos de calor e sal em sua superfície, a Corrente Circumpolar Antártica (ACC) flui continuamente para leste, ao redor do continente Antártico, formando a maior corrente oceânica do planeta, transportando cerca de 137±7 Sv ($1Sv=10^6$ $m^3.s^{-1}$) (Meredith *et al*., 2011).

Próximo ao continente Antártico, onde os ventos de leste são predominantes, existem duas correntes de grande importância, a Corrente de Talude Antártico (ASC) fluindo sobre a quebra de plataforma, e a Corrente Costeira Antártica (ACoC), sobre a plataforma continental (Figura 2). Entretanto, em regiões onde a plataforma continental é estreita, como no Mar de Weddell, a diferenciação entre a ASC e ACoC é bastante complexa (Heywood *et al*., 1998). Estas correntes determinam o regime oceanográfico ao redor do continente, pré-condicionando as massas d'água de plataforma para a formação da Água de Fundo Antártica (AABW) (Fahrbach *et al*., 1992; Heywood *et al*., 1998; Smedsrud *et al*., 2006).

Em diversos setores do Oceano Austral, como no Mar de Weddell, a ASC e ACoC atuam como uma barreira dinâmica, onde são capazes de controlar o contato da Água Profunda Cálida (WDW) com as plataformas de gelo, regulando suas taxas de derretimento basal, e por consequência, influenciando no fluxo de água doce entre a plataforma continental e as regiões oceânicas adjacentes

(Smedsrud *et al*., 2006). Neste sentido, a descrição da variabilidade espacial e temporal associada a ACoC e ASC se faz necessária para uma melhor compreensão dos processos que regem a transferência de calor, sal e *momentum* na região, e que consequentemente, influenciam o clima global.

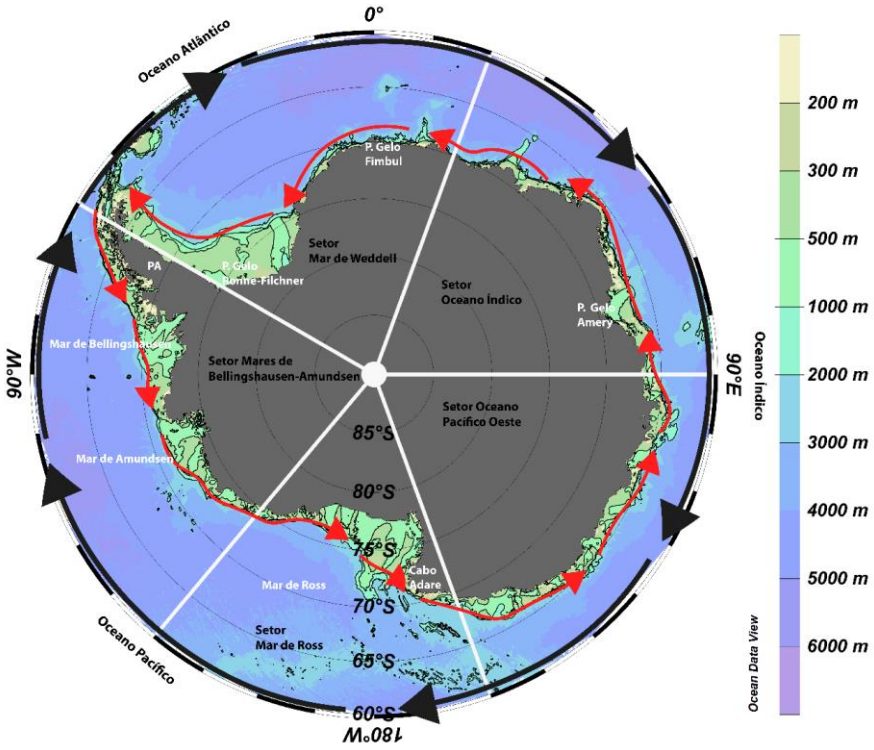

Figura 1. Setores do Oceano Austral (marcados pelas linhas brancas). As linhas pretas representam as isóbatas de 500, 1000 e 2000m. A escala de cores mostra a batimetria (Arndt *et al.*, 2013). As setas em vermelho indicam o sistema da Corrente Costeira Antártica (ACoC e ASC), enquanto que as setas em preto indicam a Corrente Circumpolar Antártica. PA= Península Antártica.

Apesar da importância do Oceano Austral na circulação oceânica global, a quantidade de amostragens nesta região continua escassa (quando comparado com regiões em menores latitudes), e ainda concentrando a maior parte da coleta de dados *in situ* durante o verão Antártico. Fora deste período, há intensa formação de gelo marinho, que dificulta a aquisição de dados através de cruzeiros oceanográficos tradicionais. Sendo assim, a utilização de fundeios oceanográficos é de extrema importância para suprir a ausência de dados nas outras estações do ano e permitir análises em um contexto temporal mais longo da variabilidade dos sistemas de correntes regionais. Neste aspecto, diversos

trabalhos vêm sendo realizados utilizando fundeios oceanográficos para investigar a ASC e ACoC.

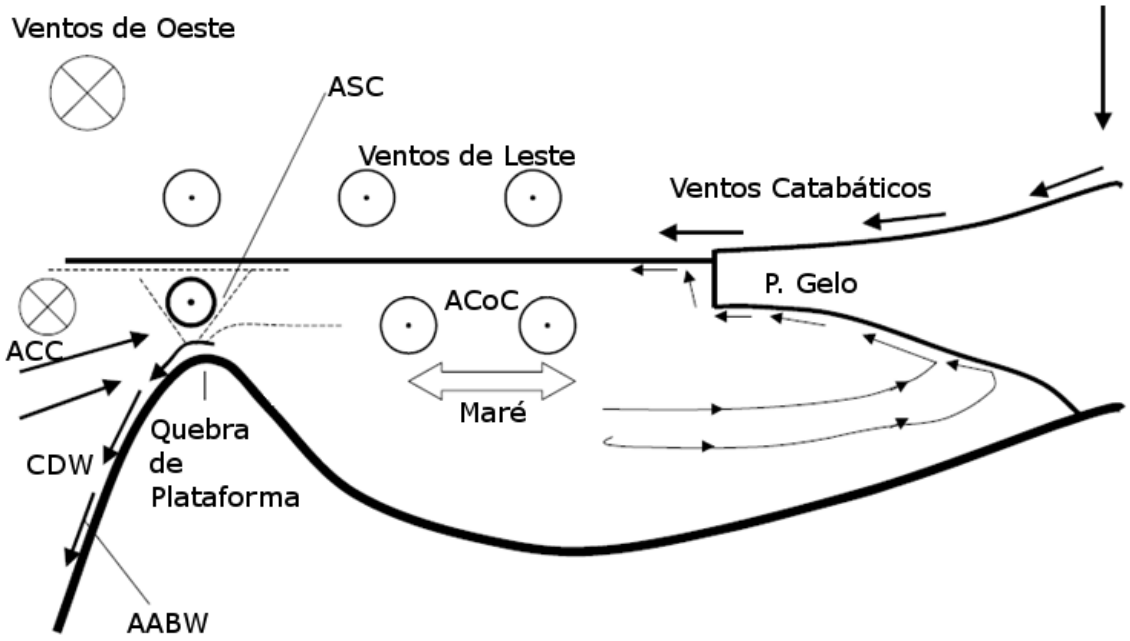

Figura 2. Esquema de uma seção vertical Norte-Sul, mostrando as principais feições da circulação próximo ao continente Antártico. AABW= Água de Fundo Antártica, ACC=Corrente Circumpolar Antártica, ACoC= Corrente Costeira Antártica, ASC= Corrente de Talude Antártico e CDW= Água Profunda Circumpolar. Adaptado de Baines (2007).

No sudoeste do Mar de Weddell, Darelius *et al*. (2009) utilizaram 20 fundeios oceanográficos, encontrando oscilações nos períodos de 35 horas, 3 e 6 dias, com uma tendência para os movimentos com períodos menores serem mais pronunciados nas regiões mais rasas. Em seu estudo à leste da região observada por Darelius *et* al. (2009), Jensen *et al*. (2013) mostraram que o modo 1 das ondas costeiras aprisionadas (CTW) foi responsável pelas oscilações de 35 horas, e que o modo 2 gerou as oscilações de 3 e 6 dias. Núñez-Riboni & Fahrbach (2009) observaram que a ACoC é 82% barotrópica, e que o vento local e a concentração de gelo marinho explicam 66% da variabilidade dessa componente.

Ao longo da frente da plataforma de gelo Amery, Herraiz-Borreguero *et al*. (2016) encontraram alta energia nas oscilações com períodos entre 3 e 8 dias, sugerindo a presença de vórtices e/ou CTW. A partir de 5 fundeios lançados em 113°E entre as isóbatas de 1000 e 4200m, Peña-Molino *et al*. (2016) observaram que o espectro da região superior do talude foi dominado por oscilações de alta frequência, com períodos menores do que 1 semana, e que nos correntômetros

próximos ao fundo da mesma região, o espectro foi dominado por oscilações entre 2 e 5 dias, períodos relacionados com CTW e vórtices de meso e submesoescala. Já nos fundeios da região inferior do talude, os espectros foram dominados por períodos entre 15 e 30 dias, que correspondem aos processos de vórtices de oceano aberto.

Na plataforma continental do Mar de Amundsen, Wählin *et al*. (2016) encontraram um pico de energia entre 40 e 80 horas, tanto nos dados de temperatura próximo ao fundo como na média vertical da velocidade, indicando que estas oscilações podem ser causadas pelas ondas topográficas de Rossby ressonantes. Também no Mar de Amundsen, Kim *et al*. (2016) mostraram que o ciclo sazonal da componente barotrópica da ACoC no Mar de Amundsen é diferente do encontrado por Núñez-Riboni & Fahrbach (2009) no Mar de Weddell, com seu máximo em outubro e mínimo em junho, enquanto que no Mar de Weddell o máximo foi encontrado em maio e o mínimo em dezembro.

Uma vez que a ACoC atua como uma barreira dinâmica na quebra de plataforma, controlando o contato das águas oceânicas com as de plataforma, o presente trabalho utilizou dados de corrente coletados a partir de 32 fundeios oceanográficos, posicionados em diversos setores da Corrente Costeira Antártica. Estes fundeios foram disponibilizados pelos programas individuais a um esforço de compilação realizado pelo SOOS (*Southern Ocean Observing System*, 2017) (Figura 3), uma iniciativa internacional que tem como principais objetivos: facilitar a implementação de um sistema de observação global e multidisciplinar para o Oceano Austral; acompanhar o desenvolvimento de novas tecnologias de observação; e unificar e intensificar as observações atuais, interagindo diversos projetos de pesquisa. Neste contexto, aproveitando a quantidade de fundeios na região de domínio da ACoC, o presente trabalho utilizou dados de velocidade a partir de instrumentos instalados em fundeios oceanográficos, com o intuito em obter uma visão circumpolar da partição de energia da ACoC em diferentes profundidades e setores ao longo da plataforma continental e talude do continente Antártico.

Figura 3. Localização dos fundeios oceanográficos lançados, recuperados e compilados pelo SOOS (Fonte: http://soos.aq/activities/soos-at-sea/moorings).

Capítulo II: Objetivos

II. 1 – OBJETIVOS

Geral

Determinar a partição espacial (vertical e horizontal) do espectro de energia no domínio da Corrente Costeira Antártica, visando identificar sua variabilidade temporal e distribuição espacial.

Específicos

- Investigar as principais escalas temporais do espectro de energia da ACoC;
- Avaliar os padrões de variabilidade nos diversos setores e profundidades da ACoC.

Capítulo III: Dados e Métodos

III. 1 – DADOS E MÉTODOS

Para analisar a partição da energia e sua variabilidade espaço-temporal, o presente trabalho utilizou dados de corrente adquiridos a partir de 32 fundeios oceanográficos (Figure 1 do manuscrito, pág 20), lançados entre 1987 e 2012, e distribuídos sobre a plataforma continental e talude do continente Antártico, disponibilizados pelos programas que participam do SOSS (*Southern Ocean Observing System*, 2017). Estes fundeios são plataformas de aquisição de dados que permanecem fixas em determinada região do oceano, podendo ser instalados diversos equipamentos, como correntômetros; sensores de pressão, temperatura e salinidade; armadilhas de sedimento, e outros (Figura 4). No total, foram analisados 59 medidores de corrente (Table 1 do manuscrito, pág 38), instalados desde 200 m de profundidade até cerca de 5 metros do assoalho oceânico, com séries temporais variando de 310 a 5354 dias.

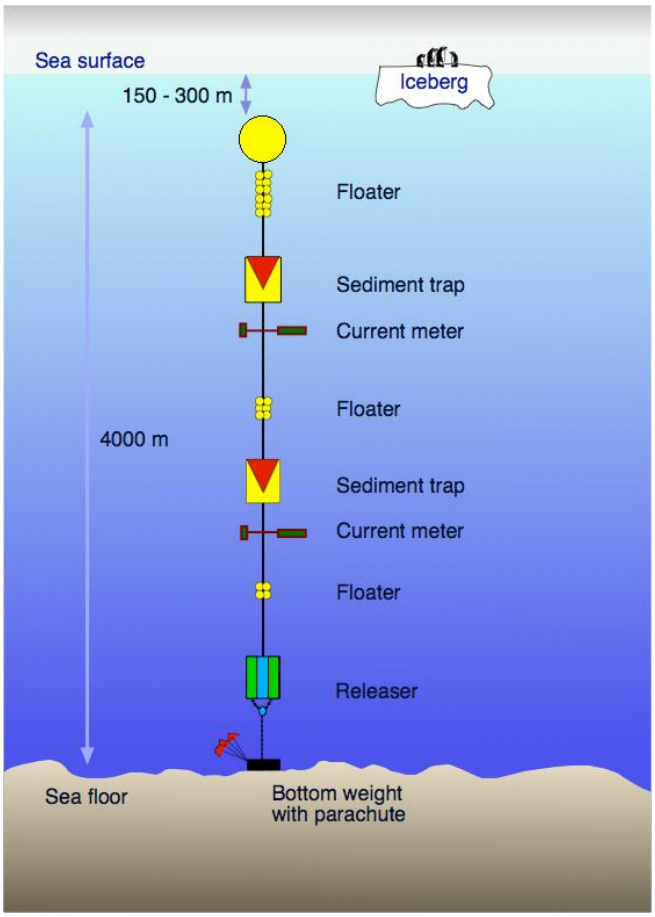

Figura 4. Exemplo de um fundeio oceanográfico com armadilhas de sedimentação e correntômetros instalados. Retirado de https://commons.wikimedia.org/wiki/File:Mooring_hg.png

Para fins de comparação vertical entre os instrumentos, a coluna d'água foi dividida em cinco camadas (Figura 5): (i) Camada Superficial, com instrumentos instalados até 300 m de profundidade; (ii) Camada Intermediária Superior, entre 300 e 600 m de profundidade; (iii) Camada Intermediária Inferior, entre 600 e 1000 m de profundidade; (iv) Camada Profunda, entre 1000 e 2000 m de profundidade; e (v) Camada de fundo, com instrumentos instalados em profundidades superiores a 2000 m. Para a análise da variabilidade espacial, a área de estudo foi dividida em cinco setores baseados na subdivisão proposta por Zwally *et al*., (2002), sendo estes: (i) Mar de Weddell, entre 60°W e 20°E; (ii) Oceano Índico, entre 20°E e 90°E; (iii) Oceano Pacífico Oeste, entre 90°E e 160°E; (iv) Mar de Ross, entre 160°E e 140°W; e (v) Mares de Bellingshausen-Amundsen entre 60°W e 140°W.

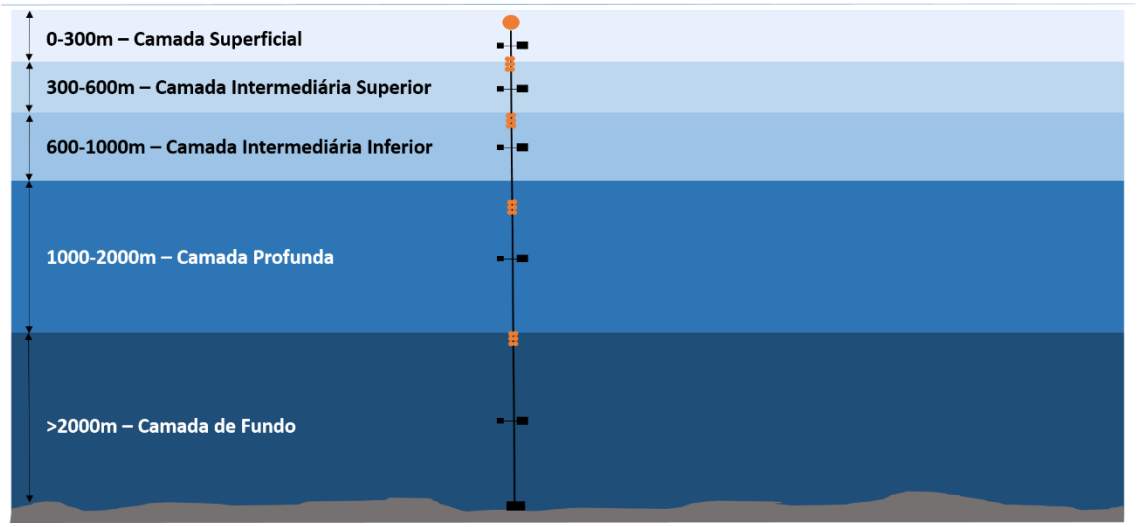

Figura 5. Esquema da divisão vertical do oceano em cinco camadas.

Os dados brutos podem conter ruídos devido à problemas com os equipamentos. Estes ruídos podem aparecer como *spikes* ou pequenas oscilações fora do comportamento normal dos dados, como problemas com o rotor do correntômetro que faz com que apareçam valores de velocidades iguais em períodos constantes (Emery & Thomsom, 2014). Desta forma, uma inspeção visual foi realizada a fim de eliminar estes ruídos. Ausência de dados em intervalos de até 6 horas na série temporal foram interpolados linearmente, enquanto que os períodos entre 6 horas e 12 dias foram preenchidos espectralmente seguindo a metodologia de Andersen (1974), como foi realizado no trabalho de Mata *et al.* (2006). Entretanto, para os correntômetros do fundeio

AWI232 instalados a 1802 e 3309 m de profundidade, encontramos um período de 30,25 dias sem dados (entre novembro e dezembro de 2005). Portanto, para não dividirmos nossa maior série temporal, este *gap* também foi interpolado espectralmente. Como estamos interessados nos eventos de baixa frequência, utilizamos o filtro passa-baixa Lanczos com frequência de corte de 40 horas para remover o efeito das marés diurnas e outras oscilações de alta frequência (Emery & Thomsom, 2014) (Figura 6).

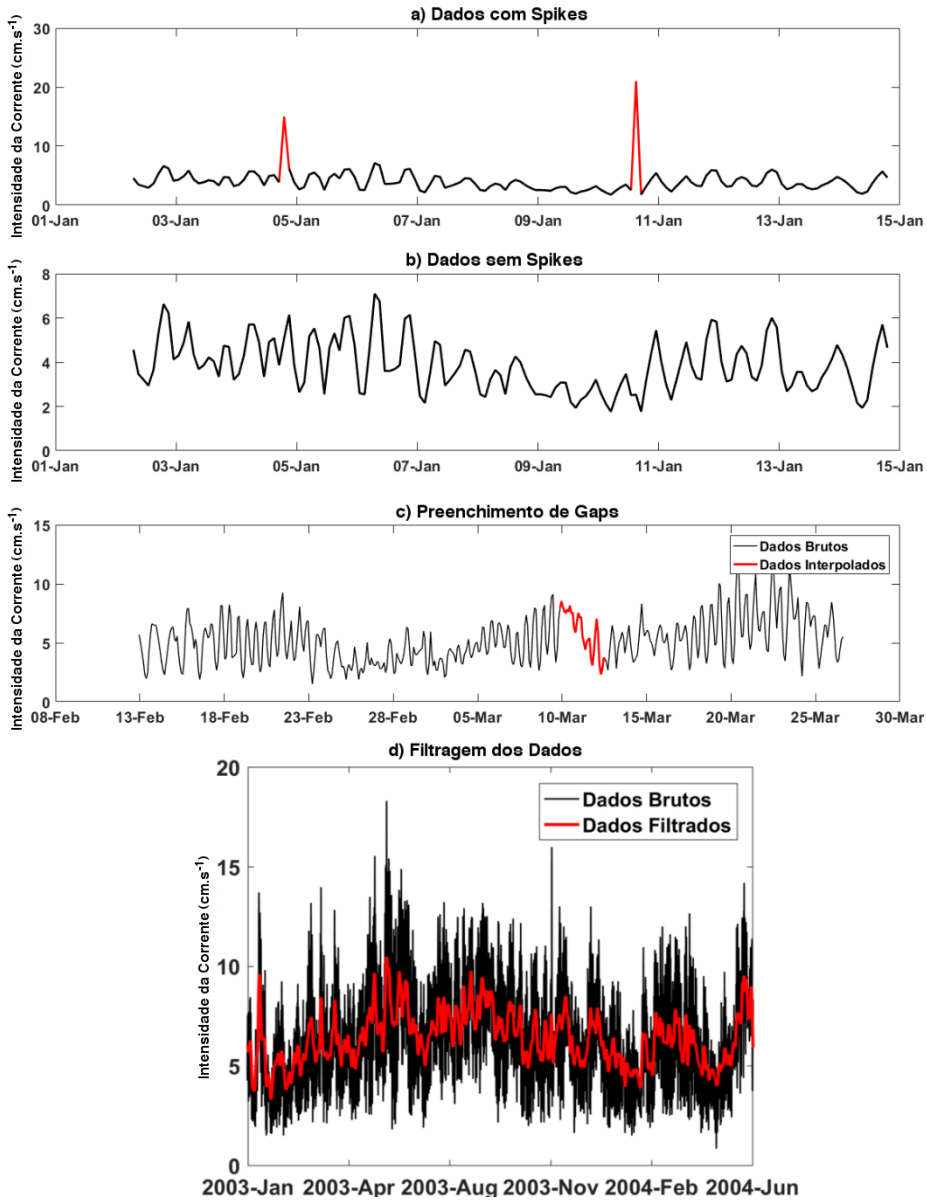

Figura 6. Exemplo da metodologia utilizada no processamento dos dados. a) Série temporal com *spikes* indicados pela linha vermelha. b) Dados após a remoção dos *spikes* e interpolados linearmente. c) Exemplo do preenchimento de *gaps* (vermelho). e) Comparação entre os dados sem filtro (preto) e os dados após o filtro passa-baixa de 40h (vermelho).

As séries temporais da velocidade da corrente contêm sinais de diversos fenômenos oscilatórios, com períodos que podem variar de dias a meses, e até anos. Sendo assim, a melhor maneira para analisar estes fenômenos é separando estes movimentos oscilatórios e identificando a amplitude de cada um através de análises espectrais. Uma vez que o método da transformada de Fourier nos mostra apenas informações da frequência sobre o conteúdo de energia, utilizamos o método das ondeletas (*Wavelets*), que nos fornece informações tanto no domínio do tempo, como na frequência (Liu & Miller, 1996) (Figura 7-a). Além disso, nas ondeletas podemos variar os parâmetros espectrais dos harmônicos ao longo da série, permitindo a observação os sinais de alta e baixa frequência simultaneamente (Torrence & Compo, 1998).

No presente trabalho, foi utilizado o método da transformada de ondeletas descrito por Torrence & Compo (1998). Entretanto, uma vez que este método superestima os sinais de menores frequências, foi aplicada a retificação proposta por Liu *et al*. (2007), a fim de aprimorar a estimativa espectral e obter uma melhor comparação entre as frequências observadas. A ondeleta *Morlet* foi escolhida como ondeleta-mãe, pois a mesma é amplamente utilizada em análises de séries temporais de dados oceanográficos (Torrence & Compo, 1998). Além da escolha da ondeleta-mãe, este método exige outros parâmetros de entrada, como o janelamento (δj=0,125), a resolução temporal (δt=0.0833 dias) e o coeficiente de defasagem (lag-1) do ruído vermelho, calculado através da autocorrelação de cada série temporal com uma defasagem de um passo de tempo.

A fim de determinar a partição de energia e a contribuição de cada banda para a variabilidade, os espectros globais das ondeletas (*Global Wavelet Spectrum*) foram integrados em cinco bandas de frequência: (i) Banda da Alta Frequência com períodos entre 40 horas e 8 dias; (ii) Banda Sinóptica, entre 8 e 20 dias; (iii) Banda da Mesoescala Superior, entre 20 e 50 dias; (iv) Banda da Mesoescala Inferior, entre 50 e 140 dias; e (v) Banda da Baixa Frequência, com períodos maiores do que 140 dias. A Figura 7 mostra um exemplo das análises dos dados após seu processamento. No espectro local de ondeletas (Figura 7-a) observamos dois eventos com alta energia (entre janeiro e agosto de 2003; e entre o fim de janeiro e o início de dezembro de 2004), com um pico em aproximadamente 52 dias. Neste sentido, com a análise de ondeletas

conseguimos avaliar não só os sinais periódicos, mas também como os mesmos variam com o tempo. O item *c* mostra a integração do espectro global das ondeletas pelas bandas de frequências definidas anteriormente. Desta forma, obtemos uma estimativa da contribuição de cada banda na partição de energia, permitindo a comparação entre diferentes regiões e profundidades.

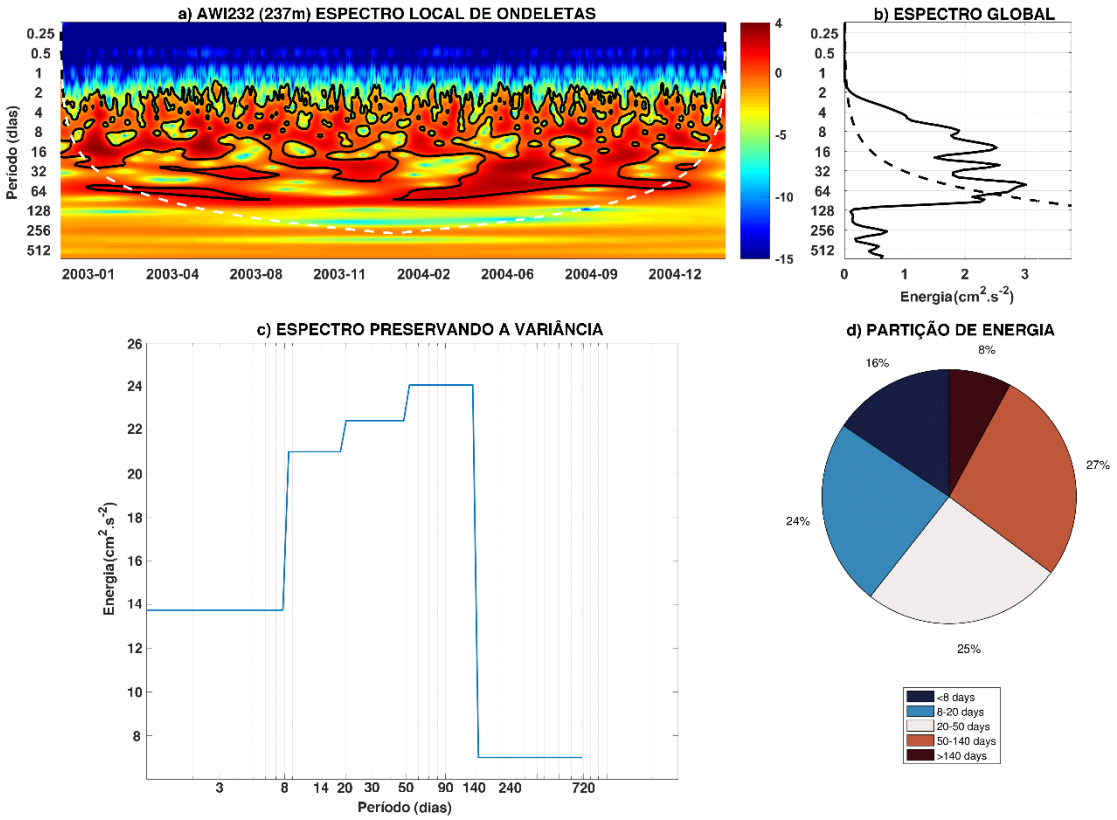

Figura 7. a) Espectro Local de Ondeletas para o correntômetro instalado à 237m de profundidade no fundeio AWI232, localizado próximo à Plataforma de Gelo Fimbul. As cores quentes indicam valores mais energéticos, onde os contornos em preto delimitam as regiões com nível de significância superior a 95%. A linha tracejada em branco limita a região do cone de influência. b) Espectro Global de Ondeletas, que mostra a análise espectral da série temporal, onde a linha tracejada em preto representa o nível de confiança de 95%. c) Espectro Preservando a Variância, indicando a partição de energia entre as cinco bandas de frequência utilizadas no presente estudo. d) Representação de *c* em forma de gráfico pizza, onde cada cor representa uma banda de frequência.

Capítulo IV: Artigo Científico

Para a obtenção do título de Mestre pelo Programa de Pós-Graduação em Oceanografia Física, Química e Geológica, é requerido que o discente realize a submissão de pelo menos um artigo científico como primeiro autor em periódico com corpo indexado. Desse modo, os resultados da pesquisa desenvolvida durante o período de mestrado e a discussão dos resultados serão apresentados em forma de artigo neste Capítulo. O manuscrito, de autoria de Rubens Torquato e Mauricio Mata, é intitulado "***A Circumpolar View of the Antarctic Coastal Current Energy Partition***".

A Circumpolar view of the Antarctic Coastal Current Energy Partition

1. INTRODUCTION

The Southern Ocean plays an important role on global ocean circulation, connecting the three major ocean basins of the planet. The mighty westerlies winds drive the largest current of the planet, the Antarctic Circumpolar Current (ACC) which flows eastward around the Antarctic continent, transporting about ±137 Sv (Meredith *et al*., 2011). South of the ACC, where the easterlies winds prevail, there are two main axis of westward flow, the Antarctic Coastal Current (ACoC), further south over the continental shelf and the Antarctic Slope Current (ASC) ruling at the shelf break. In regions where the continental shelf is narrow it is difficult to differentiate both currents (Heywood *et al*., 1998). These currents determine the oceanographic regime around the Antarctic continent, which influences several processes. For example, the dynamics associated to both of those currents help to precondition the shelf waters to the formation of the Antarctic Bottom Water (AABW) (e.g. Fahrbach *et al*., 1992, Heywood *et al*., 1998, Smedsrud *et al*., 2006). In several sectors of Southern Ocean, as in the Weddell Sea, the ACoC acts as a dynamical barrier, controlling the contact of the Warm Deep Water (WDW) with the ice shelves (e.g. Smedsrud *et al.*, 2006).

Despite the importance of these currents for global circulation, the Antarctic continental shelf and slope have been relatively poorly sampled when compared with lower latitudes. The meteorological conditions and ice cover during several months of the year lead the *in situ* observations to be mainly concentrated on summer season. Therefore, the use of moorings is important to supply the lack of observations along ice seasons and allow us to evaluate longer time series. Several studies used moorings data to investigate the ACoC and ASC, such as Núñez-Riboni & Fahrbach (2009), which revealed four driving mechanisms that determine the seasonal variability of the ACoC at the Greenwich Meridian in southern Weddell Sea. They observed the current as 82% barotropic, where the local wind and ice drag explains 66% of the current variability of this component. Other mechanisms that may cause the current variability are Sverdrup transport

and thermohaline forcing (Núñez-Riboni & Fahrbach, 2009). Also in southern Weddell Sea, Darelius *et al*. (2009) observed oscillations with periods of about 35 h, 3 days and 6 days, with a tendency of the shortest period to be stronger at the upper part of the slope. East of the site observed by Darelius *et al*. (2009), Jensen *et al*. (2013) attributed the 35 h oscillation to mode 1 of Coastal Trapped Waves (CTW) and the 3-6 days oscillation to mode 2 CTW.

Along the calving front of the Amery Ice Shelf, Herraiz-Borreguero *et al*. (2016) described the flow along the ice shelf front as an eddy-rich flow, with high energy on periods between 3 and 8 days, suggesting the presence of eddies and/or CTW. Peña-Molino *et al*. (2016) observed variability of the ASC at 113°E concentrated in periods between 2 and 5 days on the upper slope and oscillations between 15 and 30 days on the lower slope, suggesting that the upper slope is dominated by CTW and the lower by open eddy processes. At the Amundsen Sea shelf, Wählin *et al*. (2016) found a peak around 40-80h on the vertically averaged velocity and bottom temperature, indicating that these oscillations could be resonant topographic Rossby waves driven by the wind. In a close by site, Kim *et al*. (2016) studied the ACoC variability and its driving mechanisms. They found out that the seasonal cycle of the ACoC at Amundsen Sea is different from that observed by Núñez-Riboni & Fahrbach (2009) at Weddell Sea. They showed that the seasonal cycle of the barotropic component of the ACoC in Amundsen Sea had its maximum in October and its minimum in June, while in the Weddell Sea the maximum occurred in May and the minimum in December.

In spite of all these efforts, the energy partition of the ACoC system have been studied only in some specific regions and focused in a few bands of variability. Recently, the Southern Ocean Observing System (SOOS) have developed a map to aid in mooring data discovery south of 40°S (Southern Ocean Observing System, 2017). Therefore, in order to improve the knowledge of the ACoC system temporal and spatial variability, this study gives one attempt in having a circumpolar view of the temporal variability and energy partition of the ACoC system, in different depths and sectors along the Antarctic continental shelf and slope. To achieve this goal, we have used velocity time series from current meters and ADCPs installed on moorings deployed along the Antarctic continental shelf and slope. The next section will describe the data and the methods used in this

paper, followed by the description of the energy partition among five depth layers and frequency bands in the study region. Section 4 presents the general discussion, followed by the summary and conclusions which highlight the key findings of our analysis.

2. DATA AND METHODS

The dataset used in this paper is based on 32 moorings deployed around the Antarctic continental shelf and slope between 1987 and 2012 (Figure 1). The total of 58 instruments (including ADCPs and current meters) (Table 1) provided current data with the sampling rate between 10 minutes and 2 hours, placed from about 200 m depth to 5 m above the bottom. The length of the time series varied from 310 to 5354 days, but for most of the records the correspondent time series had about one-year data. To evaluate the vertical comparison among all moorings, we organized the current meters in five vertical layers as follows: the surface layer comprehends the current meters above 300 m depth; followed by the upper intermediate layer between 300 and 600 m; the lower intermediate level between 600 and 1000 m; the deep layer between 1000 and 2000 m; and the bottom level, with instruments placed below 2000 m depth. For the spatial variability analysis, we sectioned the study area into five regional sectors as described by Zwally *et al*. (2002): Weddell Sea (60°W-20°E); Indian Ocean (20ºE-90ºE); Western Pacific Ocean (90°E-160°E); Ross Sea (160°E-140°W); and Bellingshausen-Amundsen Seas (140°W-60°W).

All time series were quality controlled manually to remove most of the spikes. Short gaps (up to 6 hours) were filled linearly, while the longer ones (up to 12 days) were filled spectrally (Andersen, 1974). The only mooring with a gap longer than 12 days occurred at AWI232 current meters of 1802 and 3309 m depth with a gap of 30.25 days, time between its recovery in November and its re-deployment in December of 2005. To avoid the split of our longest time series, these data were also filled spectrally. Since we are interested in the low frequency energy band, the time series were filtered using the Cosine-Lanczos scheme with

a 40 h cut-off period, removing diurnal tides and other high frequencies oscillations (e.g. Emery & Thomsom, 2014).

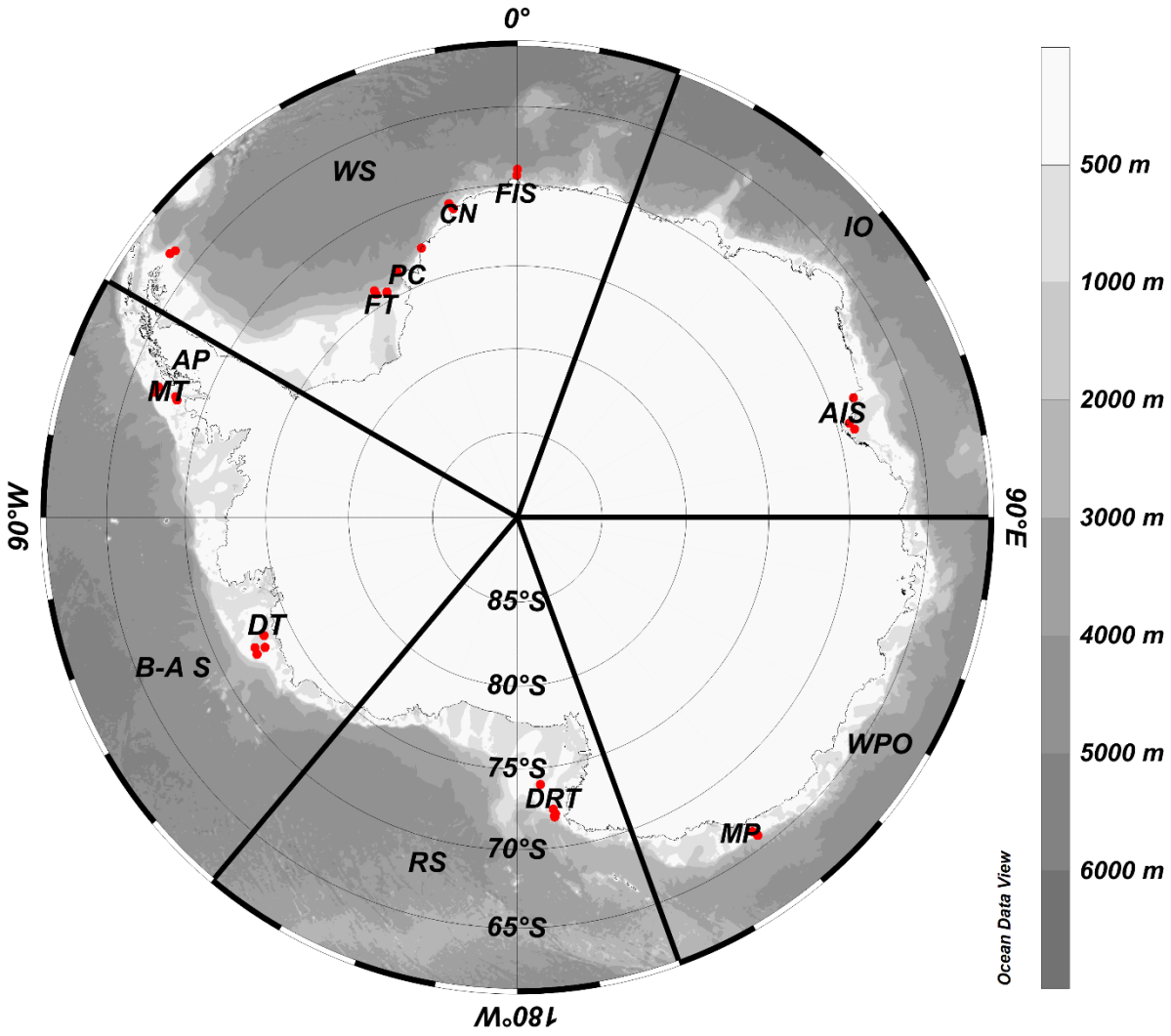

Figure 1. Map of study region showing the moorings positions (red dots). The color shading indicates the 500, 1000, 2000, 3000, 4000, 5000, and 6000m isobaths from the International Bathymetric Chart of the Southern Ocean bathymetry (Arndt *et al*., 2013). Labels represent Antarctic Peninsula (AP), Filchner Trough (FT), Polarstern Canyon (PC), Cape Norwegia (CN), Fimbul Ice Shelf (FIS), Amery Ice Shelf (AIS), Mertz Polynya (MP), Drygalski Trough (DRT), Dotson Trough (DT) and Marguerite Trough (MT). The five regional sectors are Weddell Sea (WS 60°W-20°E), Indian Ocean (IO 20°E-90°E), Western Pacific Ocean (WPO 90°E-160ºE), Ross Sea (RS 160°E-140°W) and Bellingshausen-Amundsen Seas (B-A S 140°W-60°W).

The edited time series were then decomposed into time-frequency space following the wavelet analysis tools from Torrence & Compo (1998), which is a good method to determinate the main modes of variability and also how those modes vary with time. To improve the spectral estimate and give a better comparison between the spectral peaks of the frequencies/periods, we used the wavelet power spectrum rectification proposed by Liu *et al*. (2007). In order to

evaluate the energy partition, we divided the global wavelet spectrum of each time series into five major bands: the high frequency band with periods smaller than 8 days; the weather band with periods between 8 and 20 days; the upper mesoscale which includes the periods from 20 to 50 days; the lower mesoscale with periods between 50 and 140 days; and the low frequency band with periods greater than 140 days. Since in regions with a narrow continental shelf is hard to distinct the ACoC from the ASC, in this paper all mainly westward flows (ACoC and ASC) are named as Antarctic Coastal Current (ACoC).

3. RESULTS

3.1. High Frequency Band Variability

The comparison among all layers showed the oscillations between 40 hours and 8 days as the second dominant band. At the shallow layer only the instrument at M3-Weddell mooring, placed at the continental shelf break east of the Filchner Trough had the energy partition dominated by the high frequency band. Figure 2 gives an overview of the energy distribution among the five bands of the shallow layer (instruments above 300 m depth), where the area of each pie-chart represents the total of energy (i.e. variance) and the size of the sector indicates the energy partition among our five bands.

The temporal distribution of the oscillations could be observed through the wavelet analysis, where all moorings of this layer showed high energy between the high frequency and the weather band for most of the time series. Two interesting features were observed comparing the moorings M3-Weddell and M4-Weddel (deployed ~9 km offshore of M3-Weddell): the considerable high energy at the upper mesoscale band between March and May on the M3-Weddell, which is not present at M4-Weddell; and the difference of the energy partition between both instruments. While at M3-Weddell the high frequency dominated the energy partition, at M4-Weddell the weather band was more energetic (Figure 3). However, the instruments bellow the shallow layer of M4-Weddell had more energy at the high frequency band.

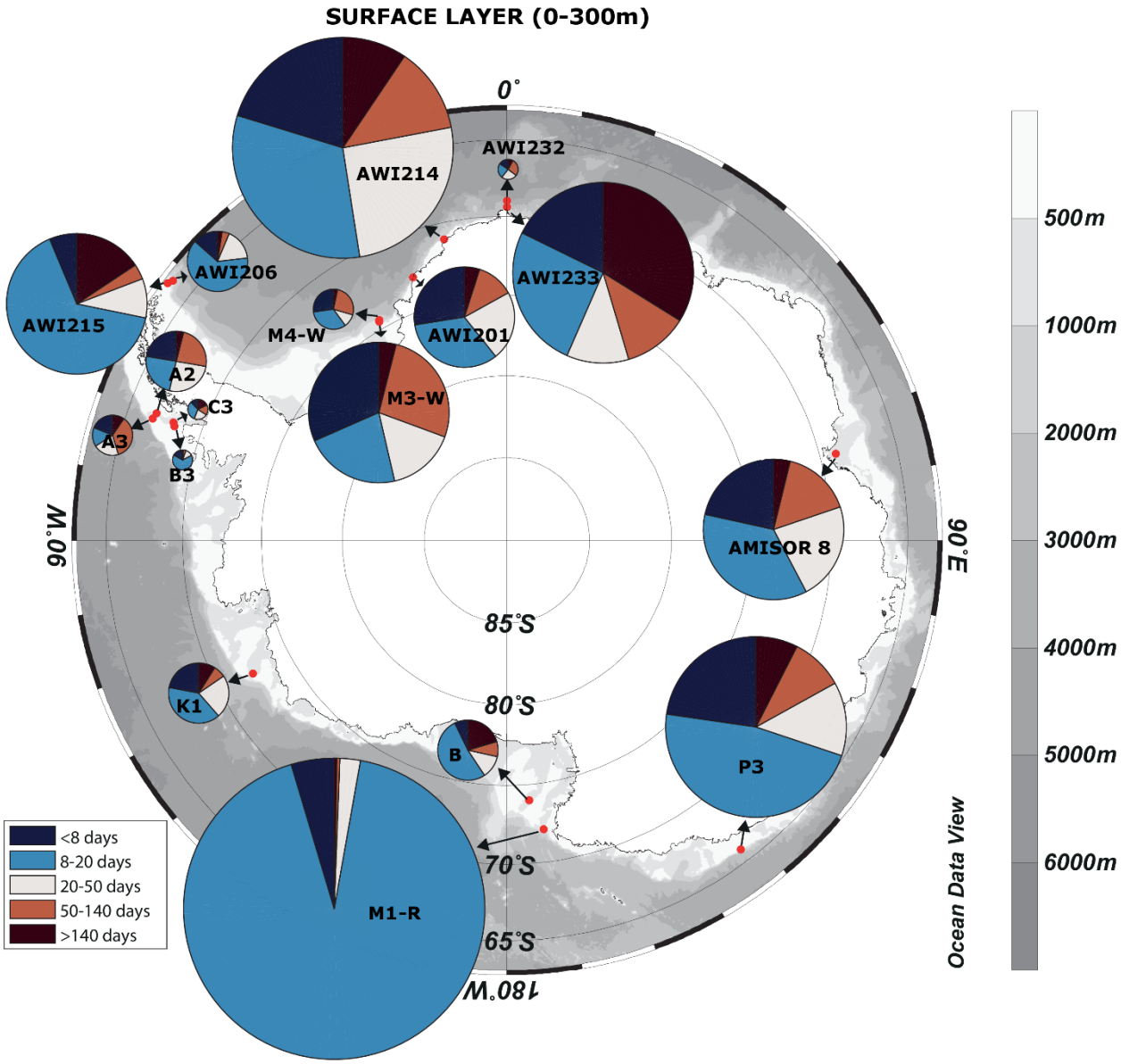

Figure 2. Energy partition among the five bands for the instruments above 300 m depth. The area of each pie-chart is proportional to the total of energy ($cm^2.s^{-2}$), where the size of the sector indicates the energy partition amongst the five bands. The red dots are the moorings position and the black arrows indicate the pie-chart for each mooring. The color shading indicates the 500, 1000, 2000, 3000, 4000, 5000, and 6000m isobaths from the International Bathymetric Chart of the Southern Ocean bathymetry (Arndt *et al.*, 2013).

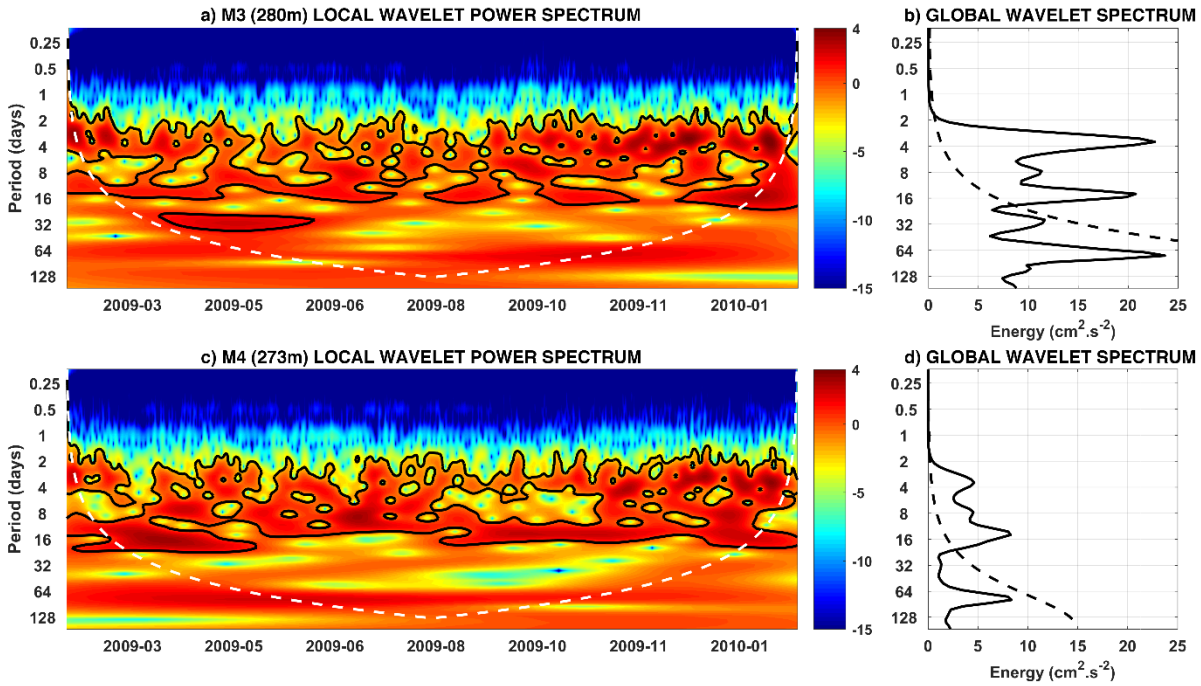

Figure 3. a) Local Wavelet Power Spectrum of the current speed for the instrument placed at M3-Weddell at 280 m depth. The black contours indicate the areas where the power is considered significant (95% confidence level), while the white dashed line is the cone of influence, where the edges effects become important. b) Global Wavelet Power Spectrum, where the dashed line is the 95% confidence level for the instrument of M3-Weddell. c) Wavelets analysis for the instrument placed at M4-Weddell mooring at 273m depth. d) Global Wavelet Power Spectrum the instrument of M4-Weddell. The color shading indicates the energy levels expressed in logarithmic scale.

In the layer with the instruments depth between 300 and 600 m, the M3-Weddell, M4-Weddell and S2 moorings had more energy at the high frequency band (Figure 4). The S2 was deployed in the Western Dotson trough and had the lowest energy (i.e. smaller pie-chart area) of the three instruments. At the instrument of M4-Weddell mooring, the energy was redistributed from the weather band (shallow layer) toward the high frequency band (300-600 m).

The level where the instruments were placed in depth between 600-1000 m, the high frequency band was the most energetic for the majority of current meters (Figure 5). Furthermore, with exception of Amisor 7 (deployed near the Amery Ice Shelf), in all moorings which this band was more energetic, the instruments were placed near the ocean floor (M3-Weddell, KN3, Amisor 2 and K2). However, at some instruments near the bottom (e.g. M1-Weddell, AWI206, M4-Ross and C3), the high frequency band did not dominate the energy partition.

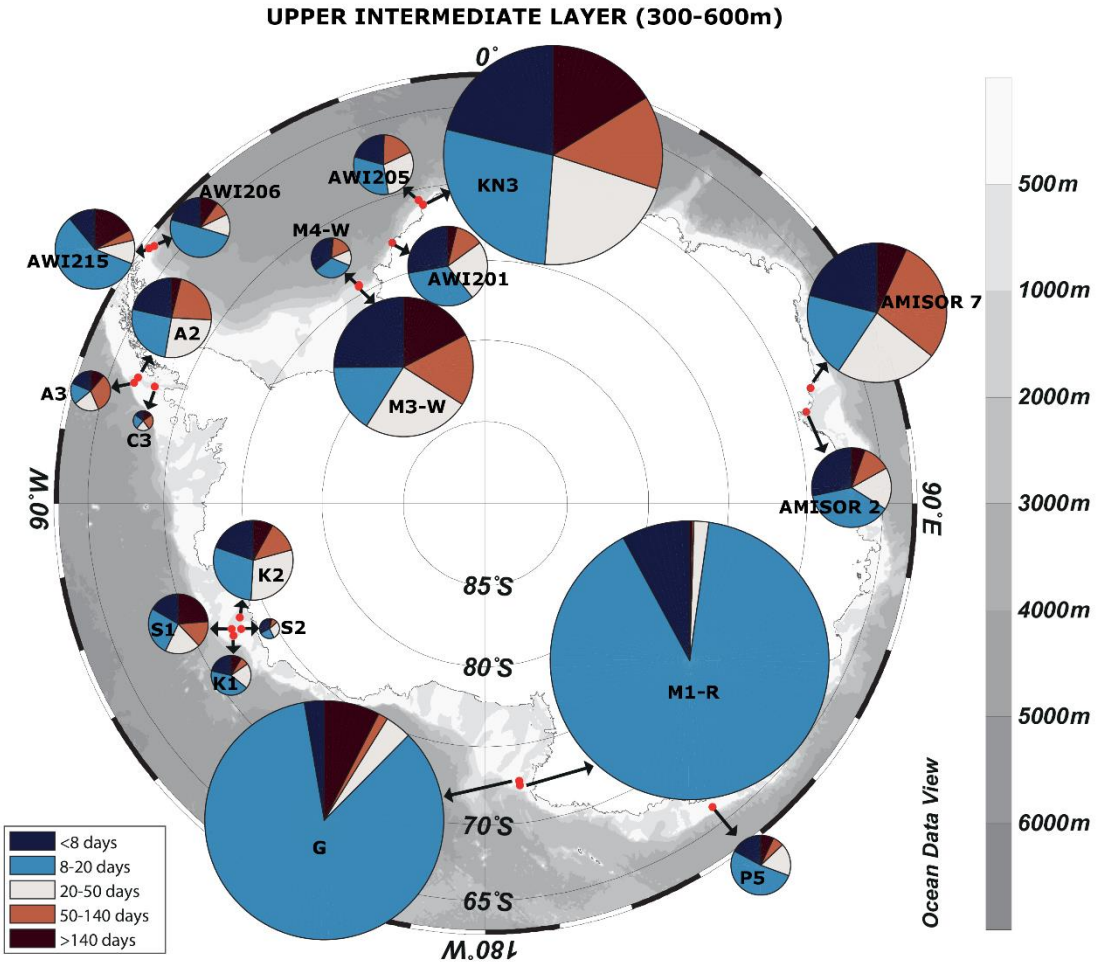

Figure 4. Energy partition among the five bands for the instruments between 300 and 600 m depth. The area of each pie-chart is proportional to the total of energy ($cm^2.s^{-2}$), where the size of the sector indicates the energy partition amongst the five bands. The red dots are the moorings position and the black arrows indicate the pie-chart for each mooring. The color shading indicates the 500, 1000, 2000, 3000, 4000, 5000, and 6000m isobaths from the International Bathymetric Chart of the Southern Ocean bathymetry (Arndt *et al*., 2013).

Between 1000-2000 m depth, the P2 was the only mooring of the Western Pacific Ocean where the high frequency band dominated the energy partition. This instrument was placed near the ocean floor in the vicinity of Mertz Polynya, with a slightly higher energy in oscillations with periods up to 8 days than at the weather band. In our deep layer, with only three instruments, all of them near the ocean floor at Weddell Sea, the high frequency band had more energy at AWI205 and AWI232.

3.2. Weather Band Variability

The energy partition among all depth layers showed that almost half of the time series analyzed had more energy at the weather band. At some sites we observe pronounced energy peaks where the weather band represents more than fifty percent of the energy partition. The great dominance of the weather band could be observed at the instruments of AWI206, AWI215, M1-Ross, B and B3 moorings at the surface layer (Figure 2); AWI206, AWI215, P5, M1-Ross, and G between 300-600 m depth (Figure 4); M4-Ross between 600-1000 m depth (Figure 5); and AWI205 and M5-Ross between 1000-2000 m (Figure 6). Despite of AWI201 and AWI205 instruments above 600 m depth, with a pronounced peak around 9-11 days, all major peaks at the weather band have occurred at the fortnightly period (~14 days) (not shown). Even when the weather band did not dominate the energy partition, this band showed a significant contribution for the current variability.

Besides the great dominance of the weather band at the AWI215 and AWI206 moorings, located in the northeast region of the Antarctic Peninsula, the contribution of energy at the high frequency band has increased with depth, showing a slightly redistribution of energy towards higher frequencies (Figure 2 and Figure 4). The opposite occurred at AWI205, placed at the continental slope near Cape Norwegia, with an increase of the contribution of energy at the weather band with depth. However, the energy of the weather band has changed from a pronounced peak around 9-11 days in depths up to 600 m to a peak at the fortnightly period in depths up to 2000 m.

The Ross Sea was the sector with the highest energy among all sites (i.e. larger pie-chart), with large peak at the fortnightly frequency in all layers up to 2000 m, specially the moorings M1 (Figure 2 and Figure 4), M4 (Figure 5) and M5-Ross (Figure 6). Like in those moorings near the Antarctic Peninsula, the only mooring with two instruments in different layers (M1-Ross), the wavelet analysis showed a slightly increase of the energy contribution of the high frequency band with depth (Figure 8).

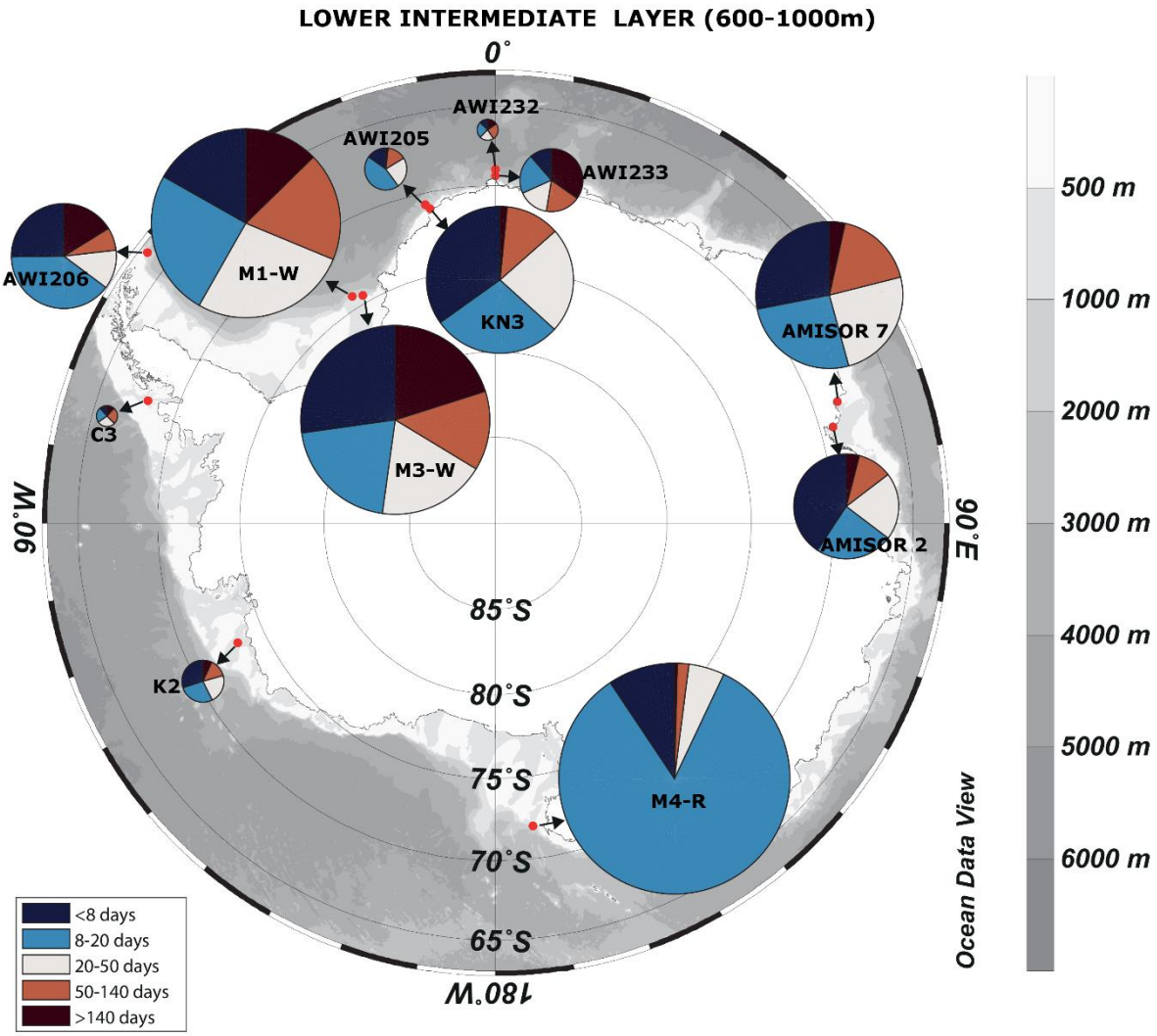

Figure 5. Energy partition among the five bands for the instruments between 600 and 1000 m depth. The area of each pie-chart is proportional to the total of energy ($cm^2.s^{-2}$), where the size of the sector indicates the energy partition amongst the five bands. The red dots are the moorings position and the black arrows indicate the pie-chart for each mooring. The color shading indicates the 500, 1000, 2000, 3000, 4000, 5000, and 6000m isobaths from the International Bathymetric Chart of the Southern Ocean bathymetry (Arndt *et al*., 2013).

3.3. Upper Mesoscale Band Variability

The oscillations between 20 and 50 days have dominated the energy partition in six moorings, four of them at the Bellingshausen-Amundsen Seas. Both instruments of A2 mooring at the surface and upper intermediate layer, deployed on the eastern side of Marguerite Trough; the instrument at depth between 600-1000 m of C3 mooring (Figure 5), deployed west of the mouth of Marguerite Bay;

and the current meter in the layer between 300-600 m depth of K2 mooring (Figure 2), deployed at Dotson Trough. At the Weddell Sea, the instrument of M1-Weddell placed at the layer between 600-1000 m (Figure 5); and the current meter of AWI213-2 of our deepest layer (Figure 7) had more energy at the upper mesoscale band. Besides the few sites with the dominance of the oscillations between 20 and 50 days, this band showed valuable contribution to the ACoC variability at some moorings.

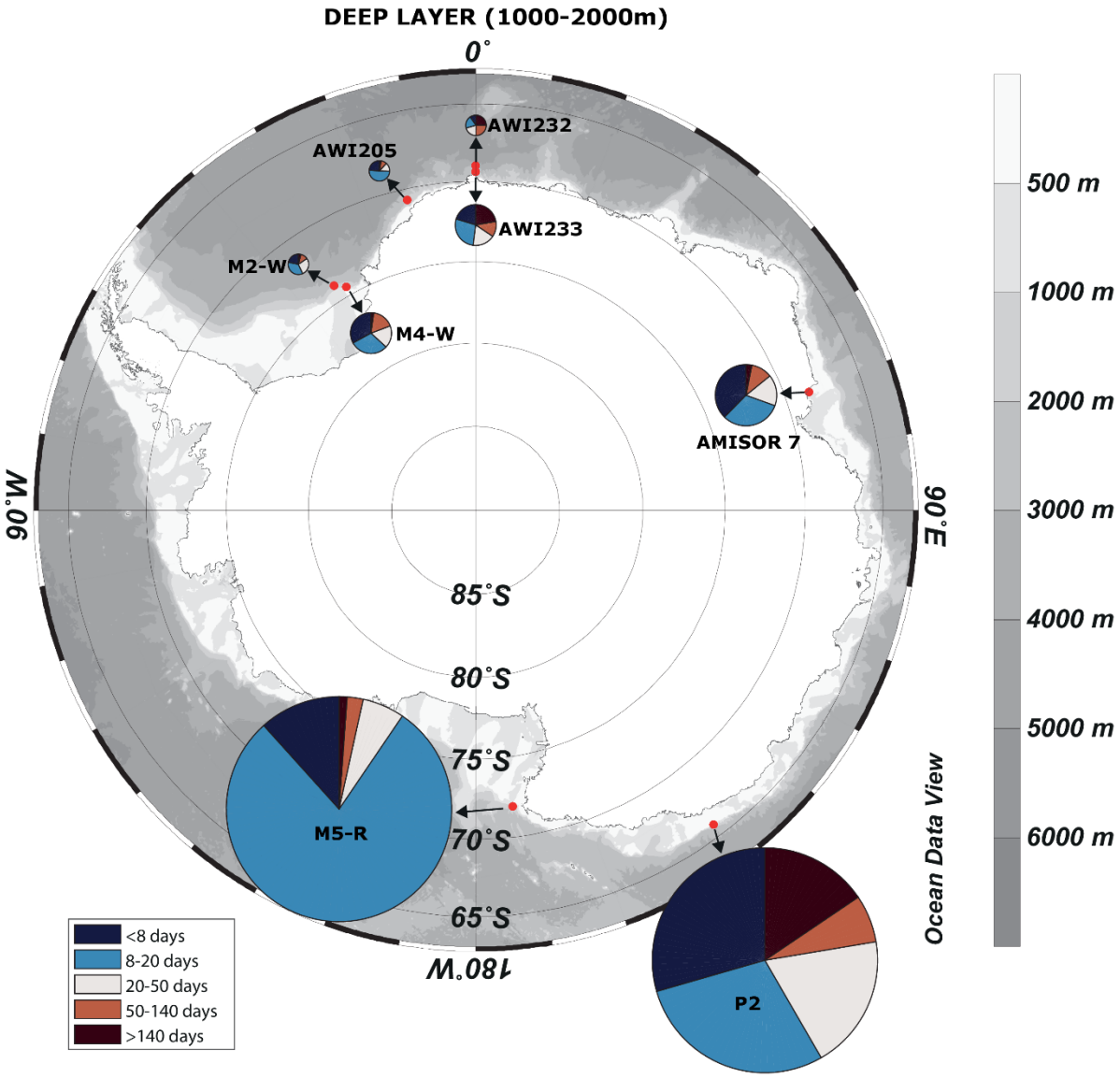

Figure 6. Energy partition among the five bands for the instruments between 1000 and 2000 m depth. The area of each pie-chart is proportional to the total of energy ($cm^2.s^{-2}$), where the size of the sector indicates the energy partition amongst the five bands. The red dots are the moorings position and the black arrows indicate the pie-chart for each mooring. The color shading indicates the 500, 1000, 2000, 3000, 4000, 5000, and 6000m isobaths from the International Bathymetric Chart of the Southern Ocean bathymetry (Arndt *et al*., 2013).

The wavelet analysis for M1-Weddell mooring, placed approximately in the middle of Filchner Trough, gives a different spectrum of the M3-Weddell, farther east. Both instruments (placed at the lower intermediate layer) had high energy on periods between the high frequency and weather band, but while at the M3-Weddell the high frequency band was more energetic, at the M1-Weddell the upper mesoscale band have dominated the energy partition (Figure 9).

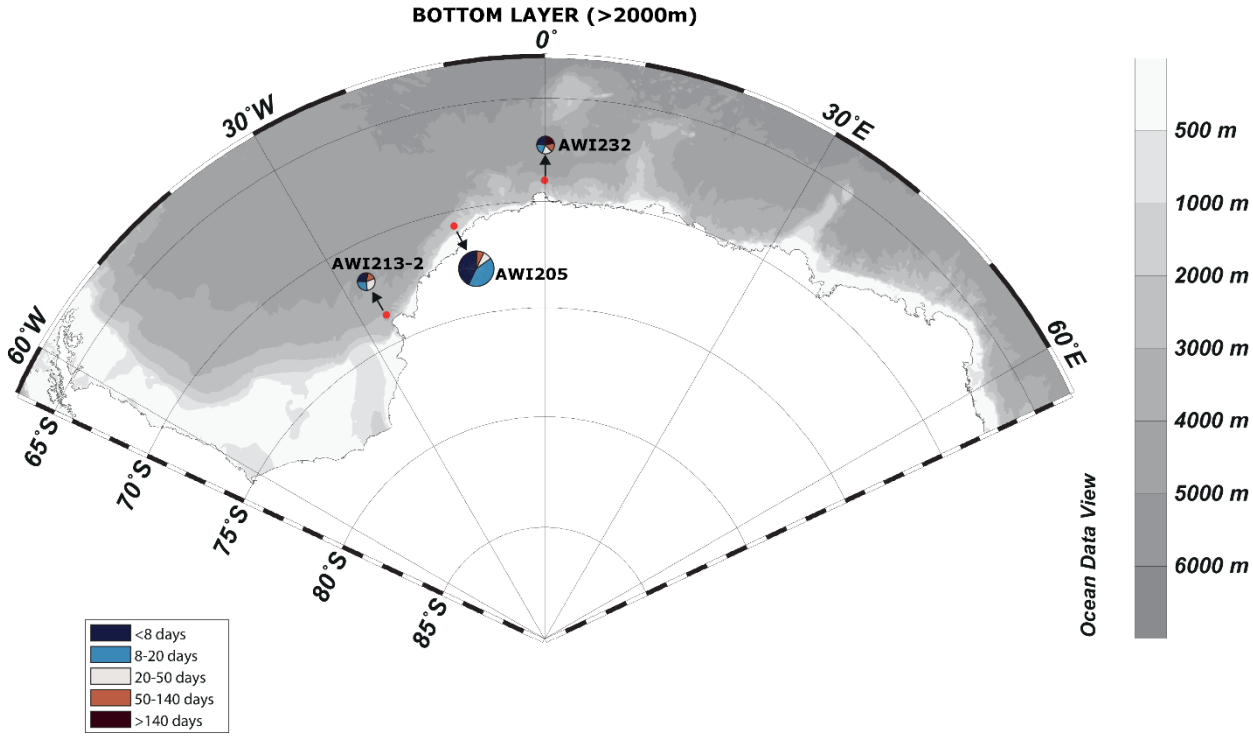

Figure 7. Energy partition among the five bands for the instruments bellow 2000 m depth. The area of each pie-chart is proportional to the total of energy ($cm^2.s^{-2}$), where the size of the sector indicates the energy partition amongst the five bands. The red dots are the moorings position and the black arrows indicate the pie-chart for each mooring. The color shading indicates the 500, 1000, 2000, 3000, 4000, 5000, and 6000m isobaths from the International Bathymetric Chart of the Southern Ocean bathymetry (Arndt *et al.*, 2013).

3.4. Lower Mesoscale Band Variability

On the surface layer, the band with periods between 50 and 140 days have dominated the energy partition at the instruments of AWI232, deployed in the lower continental slope at the Prime Meridian, and A3 mooring, placed on the outer shelf, around 45 km offshore of A2 mooring (Figure 2). The wavelet analysis of AWI232 shows two high energetic events, with a peak around 52 days from

January to August of 2003, and from late January to early December of 2004, while the A3 had one event with a major peak around 57 days from late April to early August of 2002, which explains the dominance of the lower mesoscale band to the energy partition (Figure 10). The global wavelet power spectrum of A3 instrument also shows two prominent peaks at this band, one around 90 days and other around 136 days. These peaks were also observed in the instruments placed at the upper intermediate layer for A3 and C3 moorings.

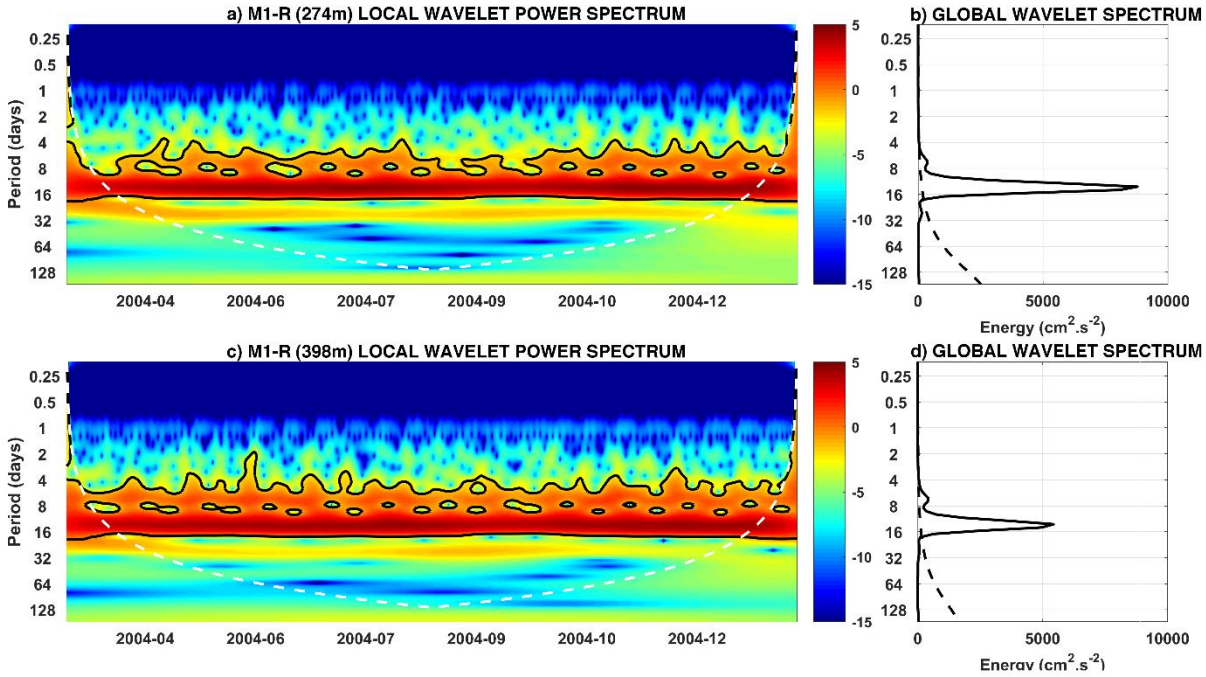

Figure 8. a) Local Wavelet Power Spectrum of the current speed for the instrument placed at M1-Ross at 274 m depth. The black contours indicate the areas where the power is considered significant (95% confidence level), while the white dashed line is the cone of influence, where the edges effects become important. b) Global Wavelet Power Spectrum, where the dashed line is the 95% confidence level for the instrument of M1-Ross. c) Wavelets analysis for the instrument placed at M1-Ross mooring at 398m depth. d) Global Wavelet Power Spectrum the instrument of M1-Ross. The color shading indicates the energy levels expressed in logarithmic scale.

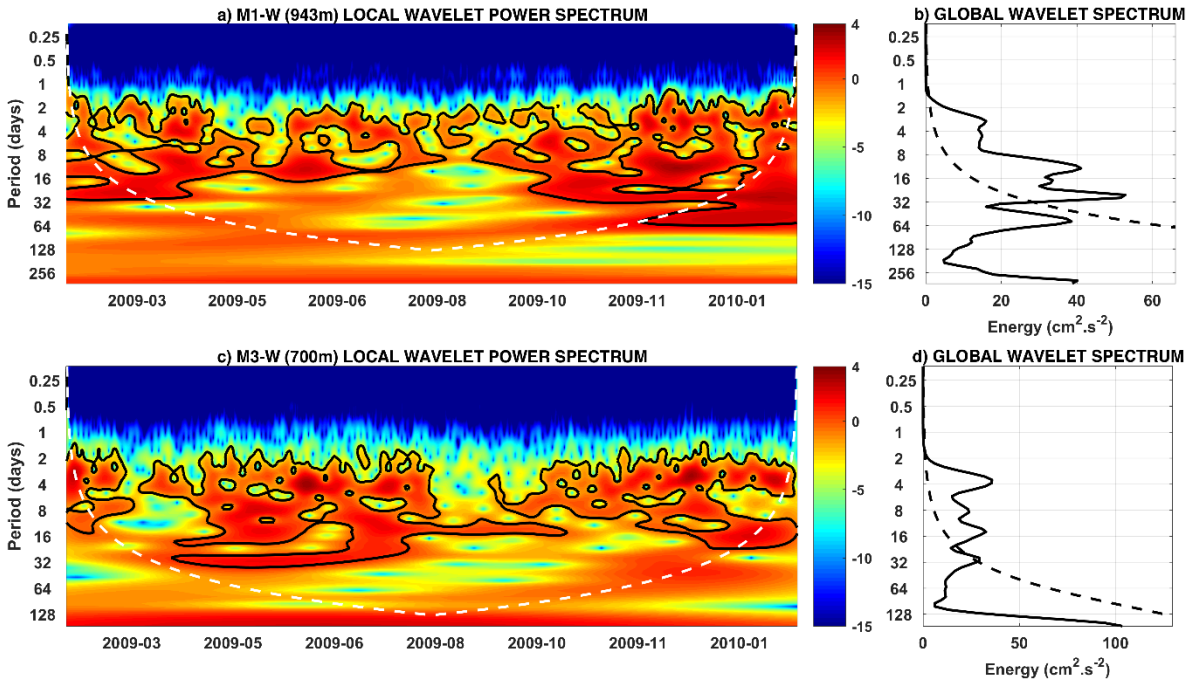

Figure 9. a) Local Wavelet Power Spectrum of the current speed for the instrument placed at M1-Weddell at 943 m depth. The black contours indicate the areas where the power is considered significant (95% confidence level), while the white dashed line is the cone of influence, where the edges effects become important. b) Global Wavelet Power Spectrum, where the dashed line is the 95% confidence level for the instrument of M1-Weddell. c) Wavelets analysis for the instrument placed at M3-Weddell mooring at 700m depth. d) Global Wavelet Power Spectrum the instrument of M3-Weddell. The color shading indicates the energy levels expressed in logarithmic scale.

3.5. Low Frequency Band Variability

Only three instruments had more energy at periods greater than 140 days, all of them deployed in the continental slope of Weddell Sea. At the surface (Figure 2) and lower intermediate layer (Figure 5), the low frequency band dominated the energy partition of the AWI233 mooring, while at the layer between 1000-2000 m (Figure 6), this band had more contribution to the variability of AWI232 mooring. However, for those instruments at AWI233 we observed pronounced peaks at this band, while for the AWI232 mooring those peaks were not prominent. Thus, the dominance of the oscillations with periods longer than 140 days at the instrument on the deep layer of AWI232 mooring could be explained by the fact of the length of the time series, where the low frequency band occupied a range up to about 2048 days.

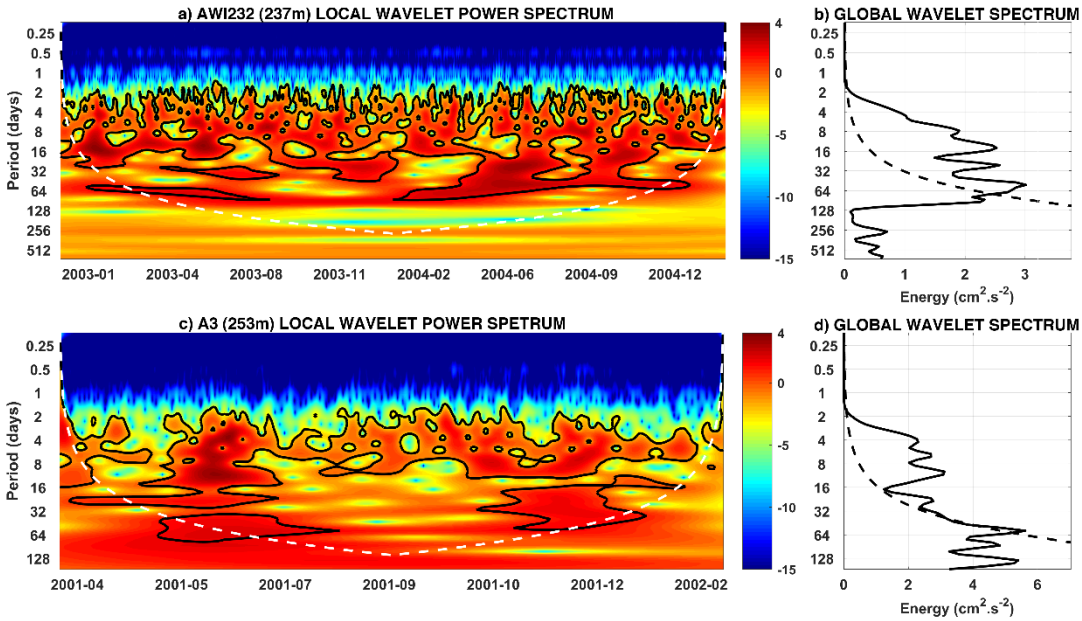

Figure 10. a) Local Wavelet Power Spectrum of the current speed for the instrument placed at AWI232 at 237 m depth. The black contours indicate the areas where the power is considered significant (95% confidence level), while the white dashed line is the cone of influence, where the edges effects become important. b) Global Wavelet Power Spectrum, where the dashed line is the 95% confidence level for the instrument of AWI232. c) Wavelets analysis for the instrument placed at A3 mooring at 253m depth. d) Global Wavelet Power Spectrum the instrument of A3. The color shading indicates the energy levels expressed in logarithmic scale.

4. DISCUSSION

4.1. High Frequency Band Variability

Using measurements of current speed from moored instruments, we observed the temporal and spatial variability of ACoC in five regional sectors of the Antarctic continental shelf and slope. As described above, the high frequency was the second dominant band among all layers, with the oscillations between 40 hours and 8 days. These frequencies have been observed in the southern Weddell Sea by Darelius *et al*. (2009) and Jensen *et al*. (2013), particularly the 3-6 day oscillations, which were attributed as the mode-2 of Coastal Trapped Waves. These are important features which can increase the heat exchange across the shelf break (Darelius *et al*., 2009; Jensen *et al*., 2013). During austral winter, Herraiz-Borreguero *et al.* (2013) observed oscillations between 2 and 8 days in temperature time series in a borehole site at Amery Ice Shelf and linked

these oscillations with the arrival of Dense Shelf Waters (DSW). Near the Amery Ice Self, using a decomposition of the velocity in axes of maximum and minimum variability, Herraiz-Borreguero *et al*. (2016) further suggested the presence of CTW and/or eddies are responsible for the oscillations between 2 and 8 days.

Our results showed a tendency of this band to be more pronounced near the ocean floor, indicating a redistribution of energy with depth to higher frequencies and thus a depth-dependence of the spectrum. However, at some sites where the instrument was placed near the ocean floor the high frequency band did not dominate the energy partition, like in the instruments of moorings M2-Weddell, AWI206, AWI215 and AWI233 at Weddell Sea; P5 at Western Pacific Ocean; and M4-Ross, M5-Ross and G at Ross Sea, where the high energetic peak at fortnightly frequency was quite important leading to the dominance of the weather band. Other instruments near the bottom had also more energy in a different band, like the M1-Weddell, AWI213-2 and C3 with more energy at upper mesoscale band. With respect of the instruments near the ocean floor, the dominance of the high frequency band at the surface and upper intermediate layers was only observed over the continental shelf break and slope of the eastern side of Filchner Trough (M3 and M4-Weddell moorings) and over continental shelf of the western side of Dotson Trough (S2). However, this band had a valuable contribution to the energy partition in most of the instruments, thus indicating an eddy/CTW rich flow as previous reported by Darelius *et al*. (2009), Jensen *et al*. (2013) and Wåhlin *et al*. (2016).

4.2. Weather Band Variability

Almost half of the instruments evaluated in this study had the energy partition dominated by the weather band, which we have defined as the periods between 8 and 20 days. These oscillations have been attributed by the weather patterns and wind stress (Middleton *et al.*, 1982). However, for most moorings this band had a prominent peak at the fortnightly frequency (~14-days period). This spring-neap tidal cycle, occurs when the K_1 and O_1 tidal components are in phase, and have been reported as an important and high energetic process, preconditioning

the export of dense water by mixing with the Modified Circumpolar Deep Water (mCDW) at the Ross Sea (Whitworth & Orsi, 2006; Padman *et al.*, 2009; Muench *et al*., 2009; Budillon *et al*., 2011). Figure 11 shows the comparison of the global wavelet spectrum among all five layers and sectors, thus indicating the high contribution of the fortnightly frequency to the variability of the weather band. In the Ross Sea, the sector with the highest energy level at this frequency, Castagno *et al*. (2017) observed the spring-neap tidal cycle on the time series of temperature and intensity of the current and linked this frequency with the mCDW intrusions. Looking at the Weddell Sea, near the Filchner overflow plume, Darelius *et al*. (2009) noticed a possible relation with the fortnightly frequency and oscillations with periods of 35 hours and 3 days, suggesting modulations in amplitude with both the high frequency and fortnightly oscillations. Flexas *et al*. (2015) indicated that the ~14 days oscillations found at the Weddell-Scotia Confluence (WSC) could be a result of the variability of the cross-slope location of the narrow high energetic along-slope current driven by processes that varies with the fortnightly modulation.

The sector with the most distinct spectral variability was by far, the Ross Sea, where all instruments had the largest total energy and a prominent peak at the fortnightly frequency. All moorings were deployed in the area of the Drygalski Trough, a region where the tidal currents can reach velocities up to 1 $m.s^{-1}$, as showed by Padman *et al*. (2009). At the tip of the Antarctic Peninsula, Von Gyldenfeldt *et al*. (2002) observed the dominance of the oscillations between 11 and 13 days over others oscillations for the AWI206 and AWI215 moorings, where the seasonal and longer period variability were hardly visible. The results showed the high importance of the spring-neap tidal cycle for the energy partition at the northeast Antarctic Peninsula (AWI215 and AWI206), west of the mouth of Marguerite Bay (B3) and Western Pacific Ocean (P3 and P5) moorings.

4.3. Upper and Lower Mesoscale Band Variability

The oscillations on both bands have been observed in the ACoC system in a few studies, like near Marguerite Trough, where the ACC flows along the outer

shelf and slope carrying both types of CDW (UCDW – Upper Circumpolar Deep Water; and LCDW – Lower Circumpolar Deep Water). Moffat *et al*. (2009) suggested the LCDW renewal on periods of about 40 days on the shelf. However, their work noticed that this time scale was subject to error due to the lack of observations on the shelf. Such oscillations have been reported as barotropic Rossby Waves at the Weddell Sea, near the Filchner Ice Shelf and in the Indian Ocean, near the region of the Amery Ice Shelf (Jensen *et al*., 2013; Herraiz-Borreguero *et al*., 2016). However, Jensen *et al*. (2013) attributed the oscillations up to 68 days as the barotropic Rossby Waves. Since those periods are linked to both our mesoscale bands, these features will be discussed together in the present section.

With exception of AWI232 and Amisor 7, all moorings with more energy at the upper and lower mesoscale band were deployed near a depression, such as the A2 (A3 and C3) placed on the eastern (western) side of Marguerite Trough (Figure 2, Figure 4 and Figure 5), M1-Weddell on the middle of Filchner Trough (Figure 5), AWI213-2 on Polarstern Canyon (Figure 7) and K2 on the middle of Dotson Trough (Figure 4). Thus, the oscillations observed near depressions should be related with the intrusions of oceanic warm waters onshore, while at the western side of the Amery Ice Shelf, this band was related with the deep convection driven by the McKenzie Polynia (Herraiz-Borreguero *et al*., 2016).

4.4. Low Frequency Variability

Oscillations with periods greater than 140 days dominated the energy partition in only 3 of the 59 instruments evaluated in this work, all of them at the Prime Meridian. Since the annual cycle has been removed for our analysis, this band can be explained by the sea ice concentration which influences the ACoC in a semi-annual cycle (Núñez-Riboni & Fahrbach, 2009), inter-annual cycle (Fahrbach *et al*., 1992) and other low frequencies modes of variability. Besides the importance of the sea ice concentration to the semi-annual variability, for most moorings the low frequency band accounts to less than 20% of the energy partition. The only instrument with a prominent peak at the semi-annual period

(with 95% confidence level) was found at the upper intermediate layer of AWI233 mooring, where the low frequency band represents 35% of the energy partition (Figure 4).

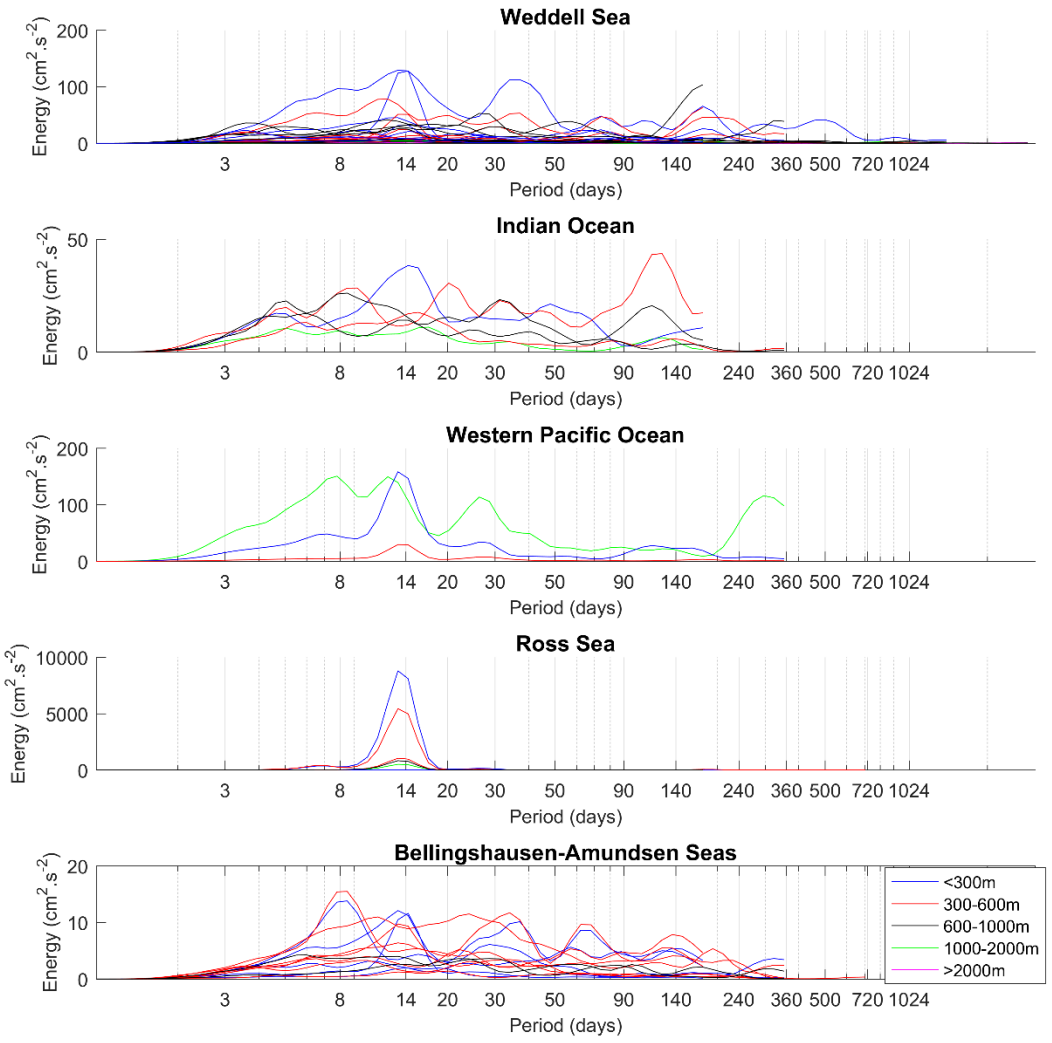

Figure 11. Global Wavelet Spectrum for all instruments for each of the five sectors. a) Weddell Sea. b) Indian Ocean. c) Western Pacific Ocean. d) Ross Sea. e) Bellingshausen-Amundsen Seas. The blue line represents the instruments placed at the surface layer (up to 300m depth), red upper intermediate layer (between 300 and 600m depth), black lower intermediate layer (between 600 and 1000m depth), green the deep layer (between 1000-2000m depth) and the magenta for those instruments placed at the bottom layer (more than 2000m depth).

The sea ice concentration modifies the surface drag coefficient impacting the momentum transfer between the wind and the current (Fennel & Johannessen, 1998). Núñez-Riboni & Fahrbach (2009) observed two periods with ACoC's

maximum speed due to the semi-annual cycle of the sea ice concentration. The first occurred in mid-autumn, with 63% of sea ice concentration, and the second in spring. However, they notice that the maximum velocity in spring was not as large as in autumn because of the relative weak wind at the spring season.

Darelius *et al*. (2016) showed that the differences of the water temperature near Filchner Trough observed between 2011 and 2013 can be explained by the differences of the wind forcing, where the weak wind found in 2013 could decrease the thermocline depth allowing a warm water inflow, reaching the Filchner Ice Shelf front. Thus, the inter-annual variability of the current could be influenced by several factors, such as the inter-annual variability of the wind stress and sea ice concentration.

5. CONCLUSIONS

The present study describes the energy partition of the Antarctic Coastal Current in a circumpolar view, from the surface layer to near the ocean floor. The Weddell Sea was the sector with the greatest mooring coverage and different patterns of variability. The oscillations between 40 hours and 8 days had a great contribution to the energy partition for most moorings, showing an eddy/CTW rich flow along the ACoC. This band dominated the partition of energy for the majority of the instruments near the ocean floor, indicating a tendency of redistribution of energy towards the high frequency with depth. However, because of the distinct peak at the fortnightly tidal cycle, the weather band was more energetic for almost half of the instruments evaluated in the present study. Furthermore, the Ross Sea, particularly the region near Drygalski Trough, had the highest total energy among all moorings, with the energy partition almost completely dominated by the fortnightly period (representing more than 80% of the total energy).

Besides the importance of the mesoscale features for the ACoC variability, only a few instruments had more energy at the mesoscale band (upper and/or lower), almost all of them near a depression, specially the Bellingshausen-Amundsen Seas moorings, where the ACC seems to flow closely to the cost, facilitating the intrusions of CDW over the continental shelf. Only one instrument

(at the upper intermediate layer near the Fimbul Ice Shelf) had more energy at the low frequency band with 95% of confidence level. This dominance occurred mainly due the prominent peak found at the semi-annual period, which have been attributed to the variability of sea ice concentration. Furthermore, some important points need to be investigated, such as the features that causes the mesoscale oscillations observed by this study and longer mooring time series are needed to investigate the inter-annual variability and other low frequency oscillations.

REFERENCES

As referências serão apresentadas no final do documento, junto com as utilizadas nos capítulos anteriores.

Table 1. Mooring details. Labels represents Alfred Wegner Institute (AWI), British Antarctic Survey (BAS), Programma Nazionale di Ricerche in Antartide (PNRA), U.S. Global Ocean Ecosystems Dynamics (U.S. GLOBEC) and Korea Polar Institute (KOPRI).

Station	Depth (m)	Instrument Depth (m)	Latitude	Longitude	Year	Recording Days	Institution	
				WEDDELL SEA				
M1	967	943	-74.2280	-32.3199	2009	365	AWI	Fer, 2016
M2	1898	1879	-73.9780	-32.2780	2009	360	AWI	Fer, 2016
M3	725	280, 530, 700	-74.5105	-30.1651	2009	361	AWI	Fer, 2016
M4	1051	273, 545, 1026	-74.4380	-30.0440	2009	361	AWI	Fer, 2016
AWI201	461	280, 380	-72.8800	-19.6250	1987	321	AWI	Krause & Rohardt, 2012
AWI205	2123	331, 796, 1550, 2090	-70.7100	-12.3583	1989	310	AWI	Fahrbach & Rohardt, 2012a
AWI206	941	246	-63.4795	-52.0962	2008	491	AWI	Fahrbach & Rohardt, 2012b
AWI206	944	490	-63.4809	-52.0970	2008	1605	AWI	Rohardt & Boebel, 2017
AWI206	944	897	-63.4809	-52.0970	2008	1956	AWI	Rohardt & Boebel, 2017

AWI213_2	3360	3330	-73.6267	-26.1167	1991	358	AWI	Fahrbach & Rohardt, 2012c
AWI214	373	198	-71.0522	-11.7178	1990	757	AWI	Fahrbach & Rohardt, 2012d-f
AWI215	460	246, 453	-63.3267	-52.7817	1996	692	AWI	Fahrbach & Rohardt, 2012g
KN3	676	390, 671	-71.0400	-11.7433	1989	366	AWI	Gerdes & Rohardt, 2012
AWI232	3353	237	-68.9978	-0.0053	2002	793	AWI	Fahrbach & Rohardt, 2012h-m
AWI232	3350	744	-68.9975	-0.0233	1996	1703	AWI	Fahrbach & Rohardt, 2012h-m
AWI232	3340	1802	-68.9963	-0.0521	1996	5354	AWI	Fahrbach & Rohardt, 2012h-m
AWI232	3333	3309	-68.9963	-0.0032	2002	2924	AWI	Fahrbach & Rohardt, 2012h-m
AWI233	1920	185	-69.3862	-0.1453	2002	1913	AWI	Fahrbach & Rohardt, 2012n-s

AWI233	1942	739	-69.3917	-0.0887	1996	4341	AWI	Fahrbach & Rohardt, 2012n-s
AWI233	1920	1802	-69.3885	-0.1258	2000	2639	AWI	Fahrbach & Rohardt, 2012n-s
				INDIAN OCEAN				
AMISOR 2	672	370, 657	-69.2000	74.0994	2001	370	BAS	Herraiz-Borreguero *et al*., 2016
AMISOR 7	1135	470, 694	-68.4776	70.3853	2001	358	BAS	Herraiz-Borreguero *et al*., 2016
AMISOR 8	717	199	-69.0003	75.3113	2001	358	BAS	Herraiz-Borreguero *et al*., 2016
				WESTERN PACIFIC SECTOR				
P2	1180	1138	-65.8012	142.9158	1998	501	BAS	Williams *et al*., 2008
P3	421	185	-65.8827	142.9248	1998	672	BAS	Williams *et al*., 2008
P5	594	568	-66.1975	143.1605	1998	671	BAS	Williams *et al*., 2008
				ROSS SEA				
M1-Ross	498	274, 398	-72.0970	172.6950	2004	331	BAS	Gordon *et al*., 2009
M4-Ross	984	964	-71.9780	172.9160	2004	330	BAS	Gordon *et al*., 2009

M5-Ross	1749	1729	-71.9070	172.9220	2004	331	BAS	Gordon *et al.*, 2009
B	607	229	-74.0034	175.0977	2012	731	PNRA	Budillon *et al.*, 2011
G	532	517	-72.3958	172.9854	2012	727	PNRA	Budillon *et al.*, 2011
BELLINGSHAUSEN-AMUNDSEN SEAS								
A2	561	247, 397	-66.8650	-70.0110	2001	320	U.S. GLOBEC	Moffat *et al.*, 2009
A3	487	253, 403	-66.7500	-71.0000	2001	319	U.S. GLOBEC	Moffat *et al.*, 2009
B3	447	247	-68.2560	-70.9980	2001	322	U.S. GLOBEC	Moffat *et al.*, 2009
C3	811	252, 395, 762	-68.1000	-70.5300	2002	365	U.S. GLOBEC	Moffat *et al.*, 2009
K1	525	250, 402	-72.3868	-117.7105	2012	670	KOPRI	Ha *et al.*, 2014
K2	823	410, 713	-73.2813	-114.9499	2012	691	KOPRI	Ha *et al.*, 2014
S1	558	401	-72.4540	-116.3489	2010	1417	KOPRI	Ha *et al.*, 2014
S2	546	400	-73.0165	-117.2490	2010	411	KOPRI	Ha *et al.*, 2014

Capítulo V: Sumário e Considerações Finais

V. 1 – SUMÁRIO E CONSIDERAÇÕES FINAIS

O presente estudo investigou a partição de energia da Corrente Costeira Antártica a partir de dados de velocidade coletados por medidores de corrente (e.g. correntômetros e ADCP's) instalados em fundeios oceanográficos sobre a plataforma continental e talude ao redor do continente Antártico. Os resultados mostram que as bandas que mais dominaram a partição de energia foram a alta frequência e a banda sinóptica. A banda da alta frequência, com oscilações entre 40 horas e 8 dias foi a segunda banda dominante, quando comparados todos os instrumentos e profundidades considerados. Esta dominância ocorreu principalmente nos instrumentos encontrados próximo ao assoalho oceânico, indicando uma transferência de energia para oscilações de alta frequência com o aumento de profundidade. Além disso, os espectros de ondeletas indicaram alta energia para esta banda em grande parte dos instrumentos, demonstrando um fluxo rico em ondas costeiras aprisionadas e/ou vórtices (e.g. Darelius *et al*., 2009; Jensen *et al*., 2013, Herraiz-Borreguero *et al*., 2016).

A banda sinóptica, com oscilações entre 8 e 20 dias dominou quase metade da partição de energia dos instrumentos analisados. Esta dominância ocorreu, principalmente devido à presença de um pico altamente energético em aproximadamente 14 dias (Figure 11 do manuscrito, pág 35), período relacionado ao ciclo de maré de sizígia e quadratura, indicando que as marés possuem grande influência na variabilidade da Corrente Costeira Antártica. Duas regiões com alta energia na frequência quinzenal foram encontradas, a primeira, próximo a depressão de Drygalski, no setor do Mar de Ross, e a segunda próximo a extremidade da Península Antártica. Em ambas as regiões foram registradas as maiores quantidades de energia total, sendo o Mar de Ross o setor mais energético, com o pico na frequência quinzenal representando mais de 80% da partição de energia. Mesmo nos instrumentos em que a partição de energia foi dominada por outra banda (e.g. alta frequência, mesoescala superior), a banda sinóptica contribuiu significativamente na variabilidade da corrente, principalmente pela a superposição das componentes de maré K_1 e O_1, que gera estas oscilações com frequência quinzenal.

Ambas bandas da mesoescala (e.g. Mesoescala Superior, com períodos entre 20 e 50 dias; e Mesoescala Inferior, com períodos entre 50 e 140 dias) foram mais energéticas em regiões próximo a depressões, principalmente no setor dos Mares de Bellingshausen-Amundsen, onde todos os fundeios foram lançados nos arredores da Depressão de Marguerite (Mar de Bellingshausen) e Depressão de Dotson (Mar de Amundsen), região em que a ACC flui mais próxima ao continente. Neste sentido, uma vez que as depressões são caminhos preferenciais para a intrusão da CDW (Dinniman *et al*., 2003), as oscilações nas bandas da mesoescala podem estar relacionadas com as intrusões de águas mais quentes provenientes de regiões oceânicas para a plataforma.

Todos os três instrumentos com mais energia na banda da baixa frequência (períodos maiores do que 140 dias) foram lançados próximo a Plataforma de Gelo de Fimbul (AWI233 e AWI232), sendo que somente um obteve um pico proeminente com 95% de nível de confiança. Este pico ocorreu no instrumento do fundeio AWI233, instalado na camada intermediária superior (entre 300 e 600m de profundidade), com alta energia no ciclo semianual, indicando que o ciclo do gelo marinho possui grande influência na variabilidade da ACoC na região deste fundeio (Núñez-Riboni & Fahrbach, 2009).

Uma vez que a ACoC possui grande importância no controle do contato entre as águas quentes oceânicas e frias da plataforma, assim pré-condicionando as águas de plataforma para a formação da AABW, pontos relevantes precisam ser melhor investigados, como as feições que imprimem os sinais observados em ambas bandas da mesoescala, lançamentos de mais fundeios em outras regiões no domínio da ACoC, e a contínua manutenção dos fundeios já existentes para aumentar o tamanho das séries temporais e assim permitir investigações de sinais com períodos maiores.

Referências Bibliográficas

Andersen N (1974) On the Calculation of Filter Coefficients for Maximum Entropy Spectral Analysis. Geophysics 39: 69–72, doi:10.1190/1.1440413.

Arndt JE, Schenke HW, Jakobsson M, Nitsche FO, Buys G, Goleby B, Rebesco M, Bohoyo F, Hong J, Black J, Greku R, Udintsev G, Barrios F, Reynoso-Peralta W, Taisei M, Wigley R (2013) The international bathymetric chart of the Southern Ocean (IBCSO) version 1.0-A new bathymetric compilation covering circum-Antarctic waters. Geophys Res Lett 40: 3111–3117, doi:10.1002/grl.50413.

Baines, PG (2007) Coastal and regional currents of Antarctica. Encyclopedia of the Antarctic. New York: Routledge, 1146.

Budillon G, Castagno P, Aliani S, Spezie G, Padman L (2011) Thermohaline variability and Antarctic bottom water formation at the Ross Sea shelf break. Deep Res Part I Oceanogr Res Pap 58: 1002–1018, doi:10.1016/j.dsr.2011.07.002.

Castagno P, Falco P, Dinniman MS, Spezie G, Budillon G (2017) Temporal variability of the Circumpolar Deep Water inflow onto the Ross Sea continental shelf. J Mar Syst 166: 37–49, doi:10.1016/j.jmarsys.2016.05.006.

Darelius E, Fer I, Nicholls KW (2016) Observed vulnerability of Filchner-Ronne Ice Shelf to wind-driven inflow of warm deep water. Nat Commun 7: 1–7, doi:10.1038/ncomms12300.

Darelius E, Smedsrud LH, Østerhus S, Foldvik A, Gammelsrød T (2009) Structure and variability of the Filchner overflow plume. Tellus, Ser A Dyn Meteorol Oceanogr 61: 446–464, doi:10.1111/j.1600-0870.2009.00391.x.

Dinniman MS, Klinck JM, Smith WO (2003) Cross-shelf exchange in a model of the Ross Sea circulation and biogeochemistry. Deep Res Part II Top Stud Oceanogr 50: 3103–3120, doi:10.1016/j.dsr2.2003.07.011.

Emery WJ, Thomson RE (2014) Data Analysis Methods in Physical Oceanography. 3ed. Elsevier, Amsterdam, 729p.

Fahrbach E, Rohardt G (2012a): Physical oceanography and current meter data from mooring AWI205. Alfred Wegener Institute, Helmholtz Center for Polar and Marine Research, Bremerhaven, PANGAEA, https://doi.org/10.1594/PANGAEA.792944

Fahrbach E, Rohardt G (2012b): Physical oceanography and current meter data from mooring AWI206-6. Alfred Wegener Institute, Helmholtz Center for Polar and Marine Research, Bremerhaven, PANGAEA, https://doi.org/10.1594/PANGAEA.792949

Fahrbach E, Rohardt, G (2012c): Physical oceanography and current meter data

from mooring AWI213-2. Alfred Wegener Institute, Helmholtz Center for Polar and Marine Research, Bremerhaven, PANGAEA, https://doi.org/10.1594/PANGAEA.792976

Fahrbach E, Rohardt G (2012d): Physical oceanography and current meter data from mooring AWI214-2. Alfred Wegener Institute, Helmholtz Center for Polar and Marine Research, Bremerhaven, PANGAEA, https://doi.org/10.1594/PANGAEA.792978

Fahrbach E, Rohardt G (2012e): Physical oceanography and current meter data from mooring AWI214-3. Alfred Wegener Institute, Helmholtz Center for Polar and Marine Research, Bremerhaven, PANGAEA, https://doi.org/10.1594/PANGAEA.792979

Fahrbach E, Rohardt G (2012f): Physical oceanography and current meter data from mooring AWI214-4. Alfred Wegener Institute, Helmholtz Center for Polar and Marine Research, Bremerhaven, PANGAEA, https://doi.org/10.1594/PANGAEA.792980

Fahrbach E, Rohardt G (2012g): Physical oceanography and current meter data from mooring AWI215-3. Alfred Wegener Institute, Helmholtz Center for Polar and Marine Research, Bremerhaven, PANGAEA, https://doi.org/10.1594/PANGAEA.792982

Fahrbach E, Rohardt G (2012h): Physical oceanography and current meter data from mooring AWI232-1. Alfred Wegener Institute, Helmholtz Center for Polar and Marine Research, Bremerhaven, PANGAEA, https://doi.org/10.1594/PANGAEA.793090

Fahrbach E, Rohardt G (2012i): Physical oceanography and current meter data from mooring AWI232-2. Alfred Wegener Institute, Helmholtz Center for Polar and Marine Research, Bremerhaven, PANGAEA, https://doi.org/10.1594/PANGAEA.793091

Fahrbach E, Rohardt G (2012j): Physical oceanography and current meter data from mooring AWI232-3. Alfred Wegener Institute, Helmholtz Center for Polar and Marine Research, Bremerhaven, PANGAEA, https://doi.org/10.1594/PANGAEA.793092

Fahrbach E, Rohardt G (2012k): Physical oceanography and current meter data from mooring AWI232-4. Alfred Wegener Institute, Helmholtz Center for Polar and Marine Research, Bremerhaven, PANGAEA, https://doi.org/10.1594/PANGAEA.793093

Fahrbach E, Rohardt G (2012l): Physical oceanography and current meter data from mooring AWI232-5. Alfred Wegener Institute, Helmholtz Center for Polar and Marine Research, Bremerhaven, PANGAEA, https://doi.org/10.1594/PANGAEA.793094

Fahrbach E, Rohardt G (2012m): Physical oceanography and current meter data

from mooring AWI232-6. Alfred Wegener Institute, Helmholtz Center for Polar and Marine Research, Bremerhaven, PANGAEA, https://doi.org/10.1594/PANGAEA.793095

Fahrbach E, Rohardt G (2012n): Physical oceanography and current meter data from mooring AWI233-3. Alfred Wegener Institute, Helmholtz Center for Polar and Marine Research, Bremerhaven, PANGAEA, https://doi.org/10.1594/PANGAEA.793098

Fahrbach E, Rohardt G (2012o): Physical oceanography and current meter data from mooring AWI233-4. Alfred Wegener Institute, Helmholtz Center for Polar and Marine Research, Bremerhaven, PANGAEA, https://doi.org/10.1594/PANGAEA.793099

Fahrbach E, Rohardt G (2012p): Physical oceanography and current meter data from mooring AWI233-5. Alfred Wegener Institute, Helmholtz Center for Polar and Marine Research, Bremerhaven, PANGAEA, https://doi.org/10.1594/PANGAEA.793100

Fahrbach E, Rohardt G (2012q): Physical oceanography and current meter data from mooring AWI233-6. Alfred Wegener Institute, Helmholtz Center for Polar and Marine Research, Bremerhaven, PANGAEA, https://doi.org/10.1594/PANGAEA.793101

Fahrbach E, Rohardt G (2012r): Physical oceanography and current meter data from mooring AWI233-7a. Alfred Wegener Institute, Helmholtz Center for Polar and Marine Research, Bremerhaven, PANGAEA, https://doi.org/10.1594/PANGAEA.793102

Fahrbach E, Rohardt G (2012s): Physical oceanography and current meter data from mooring AWI233-7b. Alfred Wegener Institute, Helmholtz Center for Polar and Marine Research, Bremerhaven, PANGAEA, https://doi.org/10.1594/PANGAEA.793103

Fahrbach E, Rohardt G, Krause G (1992) The Antarctic coastal current in the southeastern Weddell Sea. Polar Biol 12: 171–182, doi:10.1007/BF00238257.

Fennel W, Johannessen OM (1998) Wind forced oceanic responses near ice edges revisited. J Mar Syst 14: 57–79, doi:10.1016/S0924-7963(97)00018-3.

Fer I (2016): Moored measurements of current, temperature and salinity in the southern Weddell Sea, January 2009-January 2010. Geophysical Institute, University of Bergen, PANGAEA, https://doi.org/10.1594/PANGAEA.869799

Ferrari R, Wunsch C (2009) Ocean Circulation Kinetic Energy: Reservoirs, Sources, and Sinks. Annu Rev Fluid Mech 41: 253–282, doi:10.1146/annurev.fluid.40.111406.102139.

Flexas MM, Schodlok MP, Padman L, Menemenlis D, Orsi AH (2015) Role of tides on the formation of the Antarctic Slope Front at the Weddell-Scotia

Confluence. J Geophys Res C Ocean 120: 3658–3680, doi:10.1002/2014JC010372.

Gerdes D, Rohardt G (2012): Physical oceanography and current meter data from mooring KN3. Alfred Wegener Institute, Helmholtz Center for Polar and Marine Research, Bremerhaven, PANGAEA, https://doi.org/10.1594/PANGAEA.792894

Gordon AL, Orsi AH, Muench R, Huber BA, Zambianchi E, Visbeck M (2009) Western Ross Sea continental slope gravity currents. Deep Res Part II Top Stud Oceanogr 56: 796–817, doi:10.1016/j.dsr2.2008.10.037.

Ha HK, Wåhlin AK, Kim TW, Lee SH, Lee JH, Lee HJ, Hong CS, Arneborg L, Björk G, Kalén O (2014) Circulation and Modification of Warm Deep Water on the Central Amundsen Shelf. J Phys Oceanogr 44: 1493–1501, doi:10.1175/JPO-D-13-0240.1.

Herraiz-Borreguero L, Allison I, Craven M, Nicholls KW, Rosenberg MA (2013) Ice shelf/ocean interactions under the Amery Ice Shelf: Seasonal variability and its effect on marine ice formation. J Geophys Res Ocean 118: 7117–7131, doi:10.1002/2013JC009158.

Herraiz-Borreguero L, Church JA, Allison I, Peña-Molino B, Coleman R, Tomczak M, Craven M (2016) Basal melt, seasonal water mass transformation, ocean current variability, and deep convection processes along the Amery Ice Shelf calving front, East Antarctica. J Geophys Res Ocean 121: 4946–4965, doi:10.1002/2016JC011858.

Heywood KJ, Locarnini RA, Frew RD, Dennis PF, King BA (1998) Transport and water masses of the Antarctic slope front system in the eastern Weddell Sea. In Estuarine, Coastal and Shelf Science, (Elsevier Ltd), pp. 203–214.

Jensen MF, Fer I, Darelius E (2013) Low frequency variability on the continental slope of the southern Weddell Sea. J Geophys Res Ocean 118: 4256–4272, doi:10.1002/jgrc.20309.

Kim CS, Kim TW, Cho KH, Ha HK, Lee SH, Kim HC, Lee JH (2016) Variability of the Antarctic Coastal Current in the Amundsen Sea. Estuar Coast Shelf Sci 181: 123–133, doi:10.1016/j.ecss.2016.08.004.

Krause G, Rohardt G (2012): Physical oceanography and current meter data from mooring AWI201-2. Alfred Wegener Institute, Helmholtz Center for Polar and Marine Research, Bremerhaven, PANGAEA, https://doi.org/10.1594/PANGAEA.792940.

Liu, P. C., Miller GS (1996) Wavelet Transforms and Ocean Current Data Analysis. J Atmos Ocean Technol 13: 1090–1099.

Liu Y, Liang XS, Weisberg RH (2007) Rectification of the bias in the wavelet power spectrum. J Atmos Ocean Technol 24: 2093–2102, doi:10.1175/2007JTECHO511.1.

Mata MM, Wijffels S, Church JA, Tomczak M (2006) Statistical description of the East Australian Current low-frequency variability from the WOCE PCM3 array. Mar Freshw Res 57: 273–290, doi:10.1071/MF05058.

Meredith MP, Woodworth PL, Chereskin TK, Marshall DP, Allison LC, Bigg GR, Donohue K, Heywood KJ, Hughes CW, Hibbert A, Hogg AMC, Johnson HL, Jullion L, King BA, Leach H, Lenn YD, Maqueda MAM, Munday DR, Garabato ACN, Provost C, Sallée JB, Sprintall J (2011) Sustained monitoring of the Southern Ocean at Drake Passage: Past achievements and future priorities. Rev Geophys 49: RG4005, doi:10.1029/2010RG000348.

Middleton JH, Foster TD, Foldvik A (1982) Low-Frequency Currents and Continental Shelf Waves in the Southern Weddell Sea. J Phys Oceanogr 12: 618–634, doi:10.1175/1520-0485(1987)017<0784:DSWITS>2.0.CO;2.

Moffat C, Owens B, Beardsley RC (2009) On the characteristics of Circumpolar Deep Water intrusions to the west Antarctic Peninsula Continental Shelf. J Geophys Res Ocean 114: C05017, doi:10.1029/2008JC004955.

Muench R, Padman L, Gordon A, Orsi A (2009) A dense water outflow from the Ross Sea, Antarctica: Mixing and the contribution of tides. J Mar Syst 77: 369–387, doi:10.1016/j.jmarsys.2008.11.003.

Núñez-Riboni I, Fahrbach E (2009) Seasonal variability of the Antarctic Coastal Current and its driving mechanisms in the Weddell Sea. Deep Res Part I Oceanogr Res Pap 56: 1927–1941, doi:10.1016/j.dsr.2009.06.005.

Padman L, Howard SL, Orsi AH, Muench RD (2009) Tides of the northwestern Ross Sea and their impact on dense outflows of Antarctic Bottom Water. Deep Res Part II Top Stud Oceanogr 56: 818–834, doi:10.1016/j.dsr2.2008.10.026.

Peña-Molino B, McCartney MS, Rintoul SR (2016) Direct observations of the Antarctic Slope Current transport at 113°E. J Geophys Res Ocean 121: 7390–7407, doi:10.1002/2015JC011594.

Rohardt G, Boebel O (2017): Physical oceanography and current meter data from mooring AWI206-7. Alfred Wegener Institute, Helmholtz Center for Polar and Marine Research, Bremerhaven, PANGAEA, https://doi.org/10.1594/PANGAEA.875123

Smedsrud LH, Jenkins A, Holland DM, Nøst OA (2006) Modeling ocean processes below Fimbulisen, Antarctica. J Geophys Res Ocean 111: 1–13, doi:10.1029/2005JC002915.

Southern Ocean Observing System. (2017). Moorings. [online] Soos.aq. Available at: http://www.soos.aq/activities/soos-at-sea/moorings

Torrence C, Compo GP (1998) A Practical Guide to Wavelet Analysis. Bull Am Meteorol Soc 79: 61–78, doi:10.1175/1520-

0477(1998)079<0061:APGTWA>2.0.CO;2.

Von Gyldenfeldt AB, Fahrbach E, García MA, Schröder M (2002) Flow variability at the tip of the Antarctic Peninsula. Deep Res Part II Top Stud Oceanogr 49: 4743–4766, doi:10.1016/S0967-0645(02)00157-1.

Wåhlin AK, Kalén O, Assmann KM, Darelius E, Ha HK, Kim TW, Lee SH (2016) Subinertial Oscillations on the Amundsen Sea Shelf, Antarctica. J Phys Oceanogr 46: 2573–2582, doi:10.1175/JPO-D-14-0257.1.

Whitworth I, Orsi AH (2006) Antarctic Bottom Water production and export by tides in the Ross Sea. Geophys Res Lett 33: L12609, doi:10.1029/2006GL026357.

Williams GD, Bindoff NL, Marsland SJ, Rintoul SR (2008) Formation and export of dense shelf water from the Adélie depression, East Antarctica. J Geophys Res Ocean 113: 1–12, doi:10.1029/2007JC004346.

Zwally HJ (2002) Variability of Antarctic sea ice 1979–1998. J Geophys Res 107: 3041, doi:10.1029/2000JC000733.